Oriented Immobilization of Prion Protein Demonstrated *via* Precise Interfacial Nanostructure Measurements

Barbara Sanavio

SENIL
SISSA ELETTRA NanoInnovation Lab,
ELETTRA Synchrotron Light Source

Statistical and Biological Physics Sector
SISSA

A thesis submitted for the degree of

Ph.D in Statistical and Biological Physics

Academic Year 2009/2010

Abstract

Nanopatterning of biomolecules on functionalized surfaces offers an excellent route for ultrasensitive protein immobilization, for interaction measurements, and for the fabrication of devices such as protein nanoarrays. An improved understanding of the physics and chemistry underlying the device properties and the recognition process is necessary for performance optimization. This is especially important for the recognition and immobilization of intrinsically disordered proteins (IDPs), like the prion protein (PrP), a partial IDP, whose folding and stability may be influenced by local environment and confinement.

Atomic force microscopy allows for both highly controllable nanolithography and for sensitive and accurate direct detection, via precise topographic measurements on ultra-flat surfaces, of protein interactions in a liquid environment, thus different environmental parameters affecting the biorecognition phenomenon can be investigated *in situ*. Using nanografting, a tip-induced lithographic technique, and an affinity immobilization strategy based on two different histidine tagged antibodies, with high nM affinity for two different regions of PrP, we successfully demonstrated the immobilization of recombinant mouse PrP onto nanostructured surfaces, in two different orientations. Clear discrimination of the two molecular orientations was shown by differential height (i.e. topographic) measurements, allowing for the estimation of binding parameters and the full characterization of the nanoscale biorecognition process.

Our work opens the way to several high sensitivity diagnostic applications and, by controlling PrP orientation, allows for the investigation of unconventional interactions with partially folded proteins, and may serve as a platform for protein misfolding and refolding studies on PrP and other thermodynamically unstable, fibril forming, proteins.

Acknowledgements

During these intense and lively four years I've been working under the patient and encouraging supervision of prof. Giacinto Scoles (SISSA) and Dr. Loredana Casalis (ELETTRA – Sincrotrone Trieste). The work presented in this thesis has been carried out at ELETTRA, the Italian Synchrotron Light Source, with the precious and immense help of all the colleagues and friends at the SENIL (SISSA ELETTRA NanoInnovation Lab), and it is the result of a collaborative project with prof. Giuseppe Legname and his Prion Biology Lab at SISSA.

Contents

List of Figures

LIST OF FIGURES

List Of Abbreviations

AD Alzheimer's Disease, page 2

AFM Atomic Force Microscopy, page 27

AM Amplitude Modulation (AFM), page 31

BSE Bovine Spongiform Encephalopathy, page 3

CJD Creutzefeldt-Jacob Disease, page 3

CM-AFM Contact Mode Atomic Force Microscopy, page 51

CNS Central Nervous System, page 2

DDI DNA Directed Immobilization, page 18

DTT Dithiothreitol, page 15

EDC 1-ethyl-3-(3-dimethylaminopropyl)-carbodiimide, page 15

Fab antigen binding fragment of antibody, page 51

Fc constant fragment of antibody, page 18

FTLD FrontoTemporal Lobe Dementia, page 2

GMBS N-(γ-maleimidobutyrloxy) sulphosuccinimide ester, page 15

GOx Glucose Oxidase, page 46

IDPs Intrinsically Disordered Proteins, page 3

IgG Immunoglobulin G, page 38

LFM Lateral Force Microscopy, page 30

Mal maleimide, page 15

MBP Maltose Binding Protein, page 18

LIST OF FIGURES

MCHs Multivalent Chelators, page 48

MHC Major Histocompatibility Complex, page 10

NC-AFM Non Contact Mode AFM, page 30

NHS N-hydroxysuccinamidyl, page 15

NSB Non Specific Binding, page 12

PD Parkinson Disease, page 2

PDEA pyridinyldithioethanamine, page 15

PrP^{c} prion protein, cellular (physiological) form of prion protein, page 3

PrP^{sc} prion, scrapie form of prion protein, page 3

PTMs Post Translational Modifications, page 7

recMoPrP recombinant Mouse Prion Protein, page 4

recMoPrP(89-230) recombinant Mouse Prion Protein residues 89 to 230, page 4

S/N Signal to Noise ratio, page 8

SPDP 3-(2-pyridinyldithio)propioic acid N-hydroxysuccinimide ester, page 15

SPM Scanning Probe Microscopy, page 27

STM Scanning Tunneling Microscopy, page 27

STV Streptavidin, page 46

sulpho-SMCC sulphosuccinimidyl-4-(N-maleimidomethyl)cyclohexanecarboxylate, page 15

TCEP tris(2-carboxyethyl)phosphine, page 37

1

Background

The set of tools that the application of chemistry, physics and engineering, and, in particular, nanotechnology, offers to proteomics and bioanalytical chemistry is a powerful draw even for fundamental studies in the biophysics of interactions. The most fascinating property of biological system is their ability to self-assemble with remarkable specificity, robustness and predictability, and among the fundamental building block of living cells proteins are a paradigmatic example of both intramolecular (folding), and intermolecular (high-order protein architecture) self assembly. Molecular hierarchical organization, together with the capability of molecular manipulation in the size range of $1 \div 100$ nm, is the realm of application of nanotechnology. Started as a sort of molecular level foundry, nanotechnology quickly trespassed the traditional field of applied physics for energy and engineering development to open new avenues for foreground investigation of biological systems. A plethora of new techniques able to measure and manipulate submicrometric object down to the single molecule level is now available for the study of biologically relevant processes, like protein folding and protein-protein interactions.

In particular, systematic studies of protein-protein interactions have been tremendously influenced by the introduction of protein-compatible surface nanostructures on which functional and stable protein assemblies can be formed and characterized. Properly designed nanostructures combined with surface sensitive techniques, above all Atomic Force Microscopy, offer unprecedented control over active proteins immobilization at the nanoscale and their accurate biochemical characterization.

1. BACKGROUND

The overall goal of the present thesis is the development of novel routes for oriented immobilization of recombinant mouse prion protein molecules on a solid surface for further morphological and biorecognition studies. One major outcome of this research is also the expected development of effective diagnostic strategies for possible early detection of prions in prion diseases. In addition to possible diagnostics applications, the strict control over PrP orientation opens many avenues of investigation of possible interacting partners, from large macromolecular complexes to small organic dyes that interact unconventionally with unfolded proteins, and may serve as a platform for protein misfolding studies on PrP and other thermodynamically unstable proteins involved in so-called protein misfolding diseases. Among this class of maladies, neurodegenerative diseases are surmised to profit from nanotechnological based reliable detection and monitoring of molecular marker in non-invasive approaches, as well as a nanoscale sensitivity to protein conformational changes, protein interactions networks and, of course, protein fibrillation characterization.

Human neurodegenerative disorders are a broad class of pathological conditions that manifest with progressive neurological function decline. The slow but irreversible cell loss in distinct areas of the CNS (Central Nervous System) dictates the clinical presentation, as motor disorder in Parkinson Disease (PD), or cognitive impairment in Alzheimer's Disease (AD) and in Fronto Temporal Lobe Dementia (FTLD), as an example. These maladies all share remarkably similar temporal emergence patterns, even though different toxic proteins are involved in their onset. Familial neurodegenerative diseases have an earlier emergence, typically in the fifth decade of life, whereas sporadic cases do not exhibit symptoms earlier than the seventh decade.

Clinical presentation is only one part of the classical nosological classification of neurodegenderative diseases. Characterization of the anatomical regions and cell types affected, aetiology (i.e. genetic defects), and conformationally altered proteins involved in the pathogenetic process, all are instrumental in a detailed diagnosis, that in almost all cases can be confirmed only in the *post-mortem*.

Histological samples from affected tissues present insoluble but highly ordered deposits, referred to as amyloids, of specific proteins. This deposits, which high

supramolecular order is incredibly similar despite the original protein involved, arise from a structural transition, a conformational change from a physiological to an altered state that results in protein dysfunction and potentially toxic intra- or extra-cellular accumulation. Although much less is understood with regard to their function and the pathophysiological role of their misfolded conformers, a profusion of descriptive data on palpably or potentially involved proteins has accumulated and has revolutionized our knowledge on these disorders and on the protein folding problem. α-synuclein, β-amyloid, prion protein, among many others, are all neurodegenerative disease-related proteins that fall in the increasingly wide category of "Intrinsically Disordered Proteins" (IDPs). The observation that totally or partially IDPs function stems from the their natively unfolded state, in other word, from their lack of a well-defined three dimensional (3D) structure in physiological conditions, remodelled the traditional (but limited) paradigm of structure-function releationship. While proteins involved in structural and enzymatic activities are —often—distinguished for a stable folded 3D shape, IDPs seems to took advantage of their native disorder to perform regulatory, and therefore versatile, functions.

Prion disorders are invariable lethal neurodegenerative maladies that can manifest themselves in all three forms of genetic, infectious and sporadic disease. Moreover, prion diseases are probably the neurodegenerative diseases for which the largest amount of data have been collected for both humans and animals (1). Prion diseases include bovine spongiform encephalopathy (BSE) of cattle, scrapie of sheep, chronic wasting disease of deer, moose and elk (CWD), and Creutzfeldt-Jakob disease (CJD), familial fatal insomnia (FFI) and Gerstmann, Straussler and Scheinker (GSS) of humans.

The prion, PrP^{Sc},[1] consists of a conformationally altered isoform of the prion protein (PrP), a normal, membrane-anchored host protein, designated as PrP^{C}. Prion replication seems [2] to involve the direct interaction between a pathogenic PrP^{Sc} template and the endogenous cellular PrP^{C}. This interaction has been proposed

[1]The abbreviation "Sc" means *Scrapie*, the term that designated the prion disease in sheep, the first animal in which it was observed as a compulsive twitch to scratch themselves.

[2]The intervention of a possible Protein X to mediate the interaction, the misfolding, the aggregation cannot be excluded

to drive the formation of nascent infectious prions (2). PrP^C is necessary for prion replication and for prion-induced neurodegeneration, yet the proximal causes of neuronal injury and death are still poorly understood. This is one the most intriguing and peculiar characteristic of prion diseases, their ability to propagate themselves by imposing their conformation onto the cellular prion protein of the host. And the second intriguing aspect, is that the host may be not only another cell of the same organism (like in sporadic and genetic diseases), but also of another organism of the same specie (let's think at the Kuru disease transmitted through cannibalistic rituals) or from another one, as it became terribly worrisome during the widespread of BSE when the transmission to human *via* meet consumption was assessed (the vCJD). Great concern arised in the scientific community when the transmission of vCJD through blood transfusion to a recipient patient was ascertained, as current detection technique are unable to detect PrP^{Sc} at the suspected infectious concentration in blood.

To date, no effective *ante-mortem* diagnostics for prion diseases have been developed, as, among the difficulties, the infectious concentration is expected to be lower than fM in blood (3, 4, 5), below the detection limit of standard techniques like ELISA and Western Blot (6). From the above it follows that prion studies would clearly benefit from the existence of a low protein consumption nanoscale assay, such as the one presented here. Potential fields of application are *in vitro* studies investigating interactions and/or related morphological changes of PrP in native like (or physiological) conditions.

This work aim at determining the optimal nanostructure design for an Atomic Force Microscopy-based, immunoassay-like device for the oriented immbolization of recombinant mouse prion protein (residues 89-230). Recombinant (rec) mouse (Mo) PrP has been largely investigated in cellular systems and structural studies (7, 8). The discovery that recMoPrP residue 89 to 230 (hereafter recMoPrP(89-230)) can produce infectious prions when polymerized into amyloid fibrils *in vitro* has opened many new avenues of research (9) because it provides a platform for the study of prion replication *in vitro*. Nevertheless, much work remains to be carried out towards the identification of more efficient *in vitro* conversion protocols. Molecules binding to either PrP conformers may interrupt prion production by inhibiting this

interaction. Additionally, compounds that bind to supporting molecules that participate in prion production, such as chaperones or other ligands, may also be good candidates for blocking the fibril formation.

To our knowledge, very little attention has been devoted so far to the characterization of surface nanostructures of prions immobilized in a controlled orientation. On one hand, fibrillar growth has been characterized by AFM, but with little control over the orientation of the monomeric prions (10, 11). Surface based assays like ELISA or Biacore, on the other hand, have converged towards analytical devices able to study biorecognition phenomena, but without a the potential sensitivity that nanoscale control of the surface functionalization implies. Atomic force microscopy precise interfacial nanostructure measurements allows for the characterization of the antigen-antibody biorecognition phenomena on the nanostructure with unprecedented control over PrP orientation.

The achievements in prion protein oriented immobilization at the nanoscale will be preceded first by an overview of protein immobilization strategies with a particular attention to the challenges posed by nanosized structuring of interfaces. Then, an introduction to the Atomic Force Microscopy as an imaging and a nanopatternig tool will follow, in which key concepts will be depticted that are instrumental to the description of the experimental set up and the interpretation of the results.

.

2

Proteins at Nanostructured Interfaces

The extreme adaptation potential of living organisms is achieved by a finally tuned and regulated expression, in time and space, of the genome, so that system homeostasis is mantained and adapted in a concerted connection with the external environment. Protein expression is regulated right from gene activation, transcription, splicing, and translation, to folding, post translational modification (PTMs), degradation and disposal. Human genome contains 23000 genes, a considerable fraction of which –40÷60%– gives alternative splicing isoforms after transcription. To this sequence-information variability, roughly 200 different types of PTMs add additional chemical diversity, so that $\sim 10^6$ different proteins are expressed in a cell with abundances that span several orders of magnitude (12). The relative changes in specific protein content and their modifications is a signature of the cell state and therefore it is much more informative on the ongoing cellular, and eventually systemic, processes: this is the reason that boosted proteomic applications to biomarker's discovery and detection, initially for cancer(13, 14, 15), and now as a general approach to early diagnosis and personalized medicine (16, 17).

Since their introduction in 1995 (18), protein microarrays offered a route for systematic and high throughput investigation of dynamic proteome expression down to the single cell level(19, 20, 21), protein-protein interactions, protein-ligand interaction, drug screening (22) and, last but not least, novel opportunities in diagnostics

with fast, sensitive protein detection(23, 24). The requirement to monitor tiny amounts of proteins within the smallest possible detection volumes for research and diagnostics is the main driving force for the development of novel protein detection devices. Ultrasensitive measurements of proteins can be achieved "naturally" through miniaturization by nano-patterning (25, 26). Beyond high sensitivity, miniaturization also allows for parallelization, multiplexing and eventually high throughput detection schemes(6, 27, 28). Above all, however, miniaturization implies short diffusion times (that at high dilution are essential) and low sample consumption without a corresponding loss of signal-to-noise (S/N) ratio. On the other hand, regardless of the sophistication of the sensor fabrication or signal readout, the detection limits of micro- and nano-scale solid-phase arrays for protein analytes still remain well above the expected performances, which are in the attoM (10^{-18}M) and zeptoM (10^{-21}M) range (29, 30, 31).

Concerning sensitivity, current state of the art is in the low pM to fM range (6, 32). This is in contrast with the very high performance of DNA micro- and nano-detection methods in which biochemical amplification methods can be used easily and have pushed sensitivity at a level sufficient for all but the most demanding applications4, in particular early detection of tiny amount of low abundant biomarkers like prions, interleukins and hormones (though sophisticated technological improvements on single molecule enzyme-linked immunosorbent assay (ELISA) are now approaching sub-femtomolar sensitivity (33)). Nanotechnology was expected to have a much faster penetration in the diagnostics market than it actually had, since all nanoscale driven approaches to protein interaction studies are still packed in the "proof-of-principle" box. Probably, more than disobeying the "ten times cheaper, ten times better" rule of this market, the intricate mixture of sophisticated technologies and advanced competence required to operate these new procedures limited the pervasive breakthrough in biomedical sciences. Personnel indeed must be provided with proper expertise and interpretative tools for the huge and new amount of data accessible through nanotechnological application to the clinical practitioner.

So far, the accepted gold standard for single-protein measurement is immunoassay, which exploits the diversity and specificity of antigen binding by antibodies or aptamers, with the biorecognition process being governed by thermodynamic

equilibrium and suffering from time scale limitations. This becomes obvious in the typically diffusion limited reaction kinetics that may prevent the interaction to happen in practically reasonable time scales, especially at low concentrations ($<$ fM range) (32, 34, 35).

As a consequence, an improved understanding of the physicochemical characteristics of the recognition process and the properties of nanoscale protein detection devices is necessary to push and optimize their performance, particularly for the recognition and immobilization of intrinsically disordered proteins. Their folding and stability, in fact, might be easily influenced by environmental factors and the effect of local confinement.

This chapter will review briefly advantages and disadvantages of common protein immobilization chemistry, protein confinement at addressable location for microarray fabrication, and the advantages of the use of AFM both for biomolecules nanopatterning and for detection of binding events on the surface. Atomic Force Microscopy (AFM) which will be discussed throughly in the next chapter, have successfully demonstrated patterning of molecules, including stable protein structures, with sub-micrometric resolution. Moreover, the intrinsic versatility of AFM for surface biochemical studies, provides a comprehensive tool for controlled nanofabrication and subsequent investigation of the interactions between the molecules and with the interface via both height measurements and lateral deflection (e.g. molecular friction) with respect to a very flat reference substrate.

2.1 The Advantage of Measuring Protein Protein Interaction at Interfaces

Solid phases have been introduced in biomolecular interaction studies with analytical purposes almost half a century ago ((36), and see for example one early application of ELISA in human choriogonadotropin detection (37)). However, their potential in fundamental studies has been time to time re-dimensioned by an underlying skepticism about the capability of bound molecule to behave as if they were in a native environment or even to mantain their intact functionalities. In living

organism, binding events occur both in solution and at interfaces (i.e. on the cell membranes). Enzymatic reaction in the crowded cytoplasm, or in blood, and non-self antigen recognition by circulating antibodies are an example of the former case, while signal transduction events (that involves virtually all membrane bound receptor - ligand interactions), and antigen presentation by the major histocompatibility complex (MHC) are some well studied cases of the latter.

The investigation of biorecognition phenomena, the characterization of binding properties, or the use of biomolecular binding as the mean for concentration determination or analyte detection, all can then be performed in bulk or interfacial environment. Although reconstructing a platform mimicking the native landscape, in terms of environment and geometry, in which the biomolecules are usually playing their role appears to be the better choice, it is not always an easy and straightforward task, and, depending on the application field of the test, it might not be the best assay design.

Solution studies of binding parameters benefit of an isotropic distribution of the binding partners, whose diffusion constants (translational and rotational) are well-studied, a thermodynamically equilibrated boundary conditions, and an homogeneous micro-environments of binding sites, that is of special importance when nanoscale assay are involved . The major drawbacks of the traditional bulk solution approach are, beside the volumes and sample quantity involved, the difficulties in separating the bound and unbound species to quantify the actual amount of bound probes, and the lack of *in situ* monitoring of reaction kinetic rates.

Picturing the binding process, indeed, requires the accurate determination of the amount of either the free or the bound ligand, provided that a sensitive labeling technique for one of the partner is available (i.e. radioactive or fluorescent labeling) to probe the interaction, and a suitable separation technique is employed. Labeling entails separation, since the signal coming from the label is associated —generally— with the only presence of the molecule, and not with its bound or free state. Some common separation practices uses gel filtration, ultracentrifugation, ultrafiltration,

or equilibrium dialysis among others (38). The choice of the separation method relies upon kinetic consideration (or eventually raw estimation) on the mechanicistic events of binding. In particular, the lab process used to separate the bound and free state has to be fast compared to the reaction dissociation rate constant, otherwise, when the time scale are comparable, the equilibrium is disturbed by separation of the reactants.

The introduction of **heterogeneous phase assays**, in which one of the partners, the *receptor*, is linked to a sensor surface, was initially a mean for the easy spatial separation of the bound from the unbound phase in solution. Moreover, a solid substrate provides easy-handling, portability, parallelization and multiplexing. Likewise, the use of a planar substrate (in opposition to micro and nanoparticles or microporous materials) allows for the implementation of surface sensitive techniques, that can even overcome the tedious (and sometimes denaturing) practice of molecule's labeling for detection purposes, but, more intriguing, it allows for *in situ* monitoring of binding events on the surface, without any interference from the unbound molecules in the surrounding solutions.

One characteristic that distinguishes nanoscale structures from macroscopic materials is that they presents a high percentage of their constituent atoms at a surface. (The volume of an object ($V \propto l^3$, where l is the characteristic length) decreases more quickly than its surface area ($S \propto l^2$) as the size diminishes: $S/V \propto l^{-1}$, where l has atomic or molecular dimensions). This scaling behaviour leads, in the most extreme case, to structures where nearly every atom is interfacial and experience a different environment from those in the bulk (israechv,whitesides,Phillips): different free energies, electronic states, reactivities, mobilities, and structure. *Ipso facto*, interface is where gradients in properties are greatest, and so is the possibility to characterize those properties. This is both the blessing and the curse of employing nanostructured interfaces for biomolecules' interactions studies. The surface itself can be thought of as a label in the broader sense of it. Surface deposition aims at confining the molecule in an interfacial environment where it may be opportunely stabilized in time and space, and where small variation due to alternative state of the molecule immobilized —a reflection of protein activity— are enhanced and detected by surface sensitive technique. However, in common practice, the term label

is operationally defined as the attachment of a fluorescent, radioactive, enzymatic moiety that act as a reporter probe.

Immobilizing molecules on a surface enables local enrichment of the receptor with minimum sample consumption, though the high local density could actually trigger non negligible concentrations gradient of the ligand in solution, and be influenced by the binding state of the neighbouring receptors and the surrounding environment. Even when non affecting protein functionalities, the immobilization procedure itself renders the binding process mechanistically anisotropic, and, in addition, the surface may interact as a non specific binding (NSB) substrate.

2.2 Nanoscale molecular recognition interfaces

The proper surface material and surface functionalization chemistry are chosen for fabrication depending on the nature of the biological receptor, the detection methodology, and ultimately on the application for which the device is meant. Once a suitable receptor, which provides the specificity and affinity for the target analyte, is identified, the design of the molecular recognition interface involves the attachment of that receptor on a surface, and preferably its confinement to an addressable location. This linkage has to be selective enough to favour the proper orientation of the functional binding cleft, the distribution homogeneity and the degree of freedom of the tethered molecules, their lateral isotropy that turns into equality and accessibility of binding sites, and the minimization of non specific binding.

2.2.1 A Gold Standard For Planar Surfaces

Exploitation of interfacial phenomena for binding studies requires careful design of the sensor device. Among different and widely characterized possibilities, we chose ultraflat gold substrates opportunely functionalized via specific thiol/Au interaction to accomodate proteins at precise location in controlled orientation. Both the fabrication and detection steps were accomplished with the use of Atomic Force Microscopy, a scanning probe technique that can image local properties of surfaces with high spatial resolution even in liquid environment, through the control of proximity atomic interaction between a sharp probe and the surface features.

At the nanoscale, the roughness of the surface is of comparable size to the object to be studied, and might create multiple micro-environments in which the receptors and therefore the binding sites are distributed: this will affect the determination of binding parameters, since multiple binding events will take place at the same time, and an average of multiple effective binding constant will be ultimately recorded. Thus, the preparation of the gold planar surface is of utmost importance. Gold can be easily evaporated onto different substrates and grown to a polycristalline layer presenting atomically flat terraces (also referred to as Au (111) surfaces). However, for the purposes of nanosensor devices, these terraces are of too small area (below a few hundreds nanometer square), and the global roughness, expressed as root mean square deviation, may reange between 3 and 10 nm (39). Gold surfaces presenting low roughness on larger scale are produced using the Template-Stripped Gold (TSG) procedure (40) or its modified protocol by Ulman (41). Gold is evaporated on atomically flat mica, and then mechanically (or solvent) separated from it by using a flat hard surface strongly attached to the gold layer (usually, a resist is used). In this way the gold film attached to it exposes the gold surface originally buried at the interface, reproducing the flatness of mica, giving an extremely reduced roughness of about 4 Å. This is the substrated used in this thesis for the fabrication of nanostructured interfaces.

Widespread adoption of thiolate monolayer growth on gold thin films arises from the inhert nature of gold, its ample compatibility with multiple transducer technology (electrochemistry, synchrotron radiation based techniques, SPR (Surface Plasmon Resonance), AFM...), its biocompatibility, and, of course, from the well-known mechanism of spontaneous self assembly of thiols. Self assembly subsumes the spontaneous formation of complex hierarchical structures from pre-designed building blocks, typically involving multiple energy scales and multiple degrees of freedom, a peculiarity exploited and evolved by living organisms. Specifically, self-assembled monolayers are ordered molecular assemblies that are formed spontaneously by the adsorption of a surfactant with a specific affinity of its tail to a substrate, that, though often thought as planar, may be of different geometries. Since the discovery of the thiol-Au specific route by Nuzzo et al (42), an enormous variety of chemically diverse thiolated molecules have been self assembled on gold —and other metal— substrates, with extensive and detailed structural analysis of the hierarchical packed

structure of these thin films (39, 43). In addition, thiols are conveniently prepared by submerging a gold surface in a solution containing the thiol of chosen headgroup functionalization.

SAM of thiolated molecules are also a convenient way of sensor surface passivation preventing non specific protein adsorbtion out of the localized area for functionalization (44, 45). Oligoethyleneglycole (EG, three to six residues) terminated thiols are well known to protect from unspecific adsorption of biomolecules on surface. This "bioresistant" properties is common to other polymer brushes, in which flexible uncharged moieties are enriched in hydroxy groups, that, in aqueous solutions, become highly hydrated, are not ionizable under physiological conditions and protect from hydrophobic-driven denaturation (38). The exact reason for the protein resistance of EG has been subject to some debate, but it is now accepted that it is mainly due to the unusual interactions with water molecules afforded by the EG chains, creating an energetically favorable water structure which is not easily interrupted by proteins (45). In addition, steric effects and the lack of a net electrostatic charge are also likely to contribute to the protein resistance of EG-based materials.

An enormous variety of derivatized thiols are available for subsequent surface chemistry, like protein functionalization. The way this functional group is introduced in the SAM range from presenting a mixed solution to the gold, to micro- and nano-patterning of the desired molecule, and will be reviewed in a following section.

2.2.2 Protein Immobilization Techniques

Protein immobilization at the micro and nanoscale has evolved in the latest years from simple and less effective physical adsorption to sophisticate combination of non covalent and covalent chemistries.

2.2.2.1 Physical adsorption of proteins

Protein physisorbtion relies on non-selective ionic, van der Waals, electrostatic and hydrophobic interactions of the protein molecules with the hosting surface. The strength of the interactions may be enough to stabilise the immobilization of the proteins on the surface, that, however, lie in an unhomogeneous and uncontrolled

orientation, and are prone to time-dependent, slow thermodynamically-driven unfolding (due to the spontaneous tendency to increase the amount of hydrophobic contact between the polypeptide and the surface and minimize the interfacial interaction energy).

This non selective hydrophobic or electrostatic driven interaction between polypeptides and surfaces is actually the basis also for non specific —and therefore, undesired— adsorption of proteins to biochips and, in general, to biocompatible micro- and nano-structured materials, and is of great interests for prosthetic material and drug delivery optimization. Effects like the **protein corona**, that is the decoration of nanoparticles with endogenous proteins as they circulate in the bloodstream, or unspecific background in microwell and microarray test modify their performances.

2.2.2.2 Covalent immobilization of target molecules

Covalent linking of proteins offers the enormous advantage of a very stable functionalized surface over time. Proper functional moieties are located on the surface to react with, possibly a few, residues of the protein to be immobilized. Chemistries which allow direct coupling to amino acid residues are generally preferred due to their universal applicability. The mostly used examples are depicted in figure 2.1 and include N-hydroxysuccinimide (NHS), imidazole carbamate, epoxide and aldehyde groups, which may react with lysine residues, and various thiol-reactive chemistries, which may react with free cysteine residues. Antibody immobilization benefit also of chemistry targeting post translational modifications like the glycosilation moieties, or disulfide bridgs.

It is very common to exploit the reactivity of activated carboxylic groups towards free amino groups, since it is a highly generalizable procedure and works easily both on purified and recombinant proteins (which may lack organism specific PTMs). Carboxylic groups can be patterned onto the surface, and then activated through carbodiimide and NHS to react with ϵ amino groups in lysine side chains, as it will be also shown in chapter 4 for an alternative recMoPrP immobilization strategy.

Standard covalent cross-linking strategies does not usually provide any selective reactivity. Therefore, the resulting protein layer is heterogeneous in orientation and

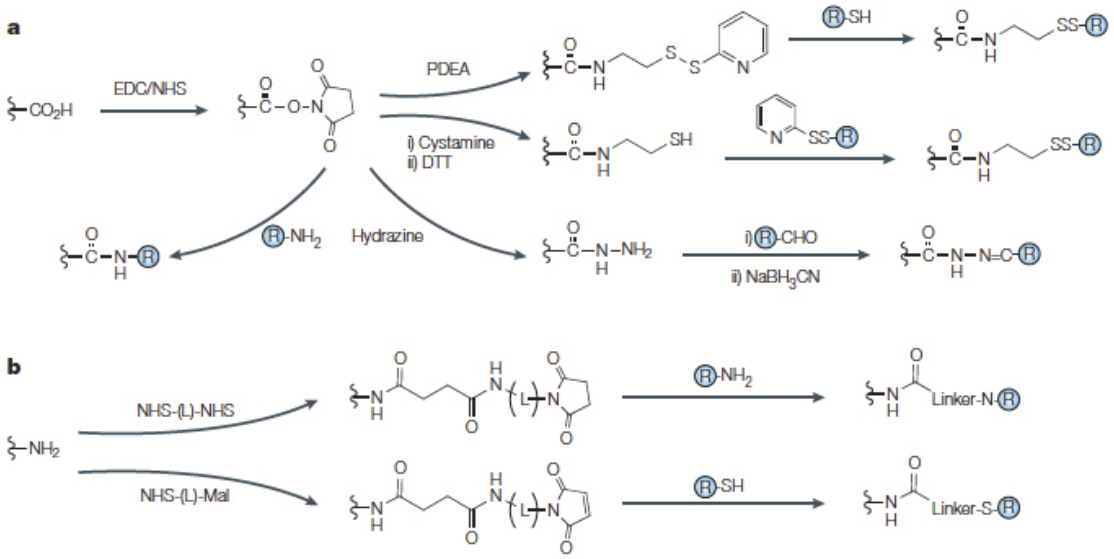

Figure 2.1: **Common covalent chemistries for protein immobilization** - a) Water-soluble EDC-mediated activation of a **carboxylic group** on the support. The resultant reactive NHS ester can then be coupled directly with available amino moieties of a receptor (R) to form a stable amide linkage. Alternatively, subsequent activation steps allows for a variety of other coupling. Derivatization with sulphydryl-reactive reagents (PDEA or SPDP) allows reaction with free surface thiols (for example, cysteine or methionine). Stable thioether bonds can be formed using maleimide coupling reagents, such as sulpho-SMCC and GMBS. The surface can also be derivatized with cystamine to effect coupling with disulphide-activated proteins. Finally, treatment with hydrazine followed by a reductive amination allows coupling with aldheydes. b) Amino-presenting surfaces can be treated with bifunctional linking reagents for coupling with free amino or sulphydryl groups on the protein. Adapted from (46)

function, and is likely to have an heterogeneous response to any stimulus applied, including an heterogeneous binding behaviour, decreasing the overall performances of the device.

Recent applications of site specific covalent immobilization like Staudinger ligation, click-chemistry, copper free click chemistry, and derived protocol suitable to non denaturing protein immobilization, all step forward for reliable orientation-selective linking. However, many of these protocols involve the reaction of the functional moieties on the surface with an activated protein, that is, a protein chemically functionalized with a suitable reactive linker. Some of this linker can be genetically encoded in few cases in recombinant protein (i.e. tioesther groups). This protocol requires some expertise, and up to know much of the applications are relative to model synthetic peptides and very rarely to native proteins [1].

A straightforward and convenient route for direct, site specific immobilization of proteins and peptides takes advantage of the specific reaction between cysteine thiols and gold. As it will be shown in chapter 3 (section 3.3.2), protein can be engineered with a double cysteine tag (**Cys_2-tag**) in known position (either the N-terminal or C-terminal side), allowing for site specific covalent linking. The only drawback of this approach, compared to other fusion peptide described later on, is that in some cases folding might be affected. In fact, proteins which folding is stabilized by disulfide bridges between native cystein residues may form non native disulfide bonds with the additional cysteines of the cys-tag.

2.2.2.3 Biochemical affinity immobilization

Bioaffinity non covalent immobilization (49, 50) exploits the specificity and the affinity of biomolecules for some particular ligands, and provides not only oriented and homogeneous attachment but also the possibility of detaching the protein and thus repeated use of the same surface. The kind of biochemical affinity used involves antibody antigen interactions, immobilized metal affinity, substrate-receptor affinity. Many protein can be recombinantly engineered with a proper tag that brings the suitable affinity interaction for oriented immobilization. Concerning antibody

[1] Recent and detailed overview o these novel chemistries and their application can be found in (47, 48)

immobilization, they can be used to orient their antigen on the surface, provided their binding site is oriented too.

- **Avidin-biotin based systems** make use of the strongest noncovalent known binding affinity between streptavidn and biotin ($K_d = 10^{-15}M$). Biotin labeling of molecules (which can be achieved through reaction with maleimido or carboxylic activated groups) ensures a tight and stable surface derivatization.

- **Protein A immobilization** is based on the high affinity and binding specificity of Protein A, a surface protein of *Staphylococcus aureus*, towards the Fc region of a broad range of mammalian immunoglobulins (Ig). Protein A layer are immobilized, *via* affinity capture, physical adsorption or covalent coupling to a surface, and then the IgG layer is captured in an oriented manner.

- **Fusion proteins** are engineered to encode in one polypeptide chain the protein of interest and a fusion tag, used for chemical linking to the surface *via* affinity for a specific substrate (38). Many of this fusion system have been extensively studied for protein purification purposes. Glutathione S-Transferase (GST) binds to surface-immobilized glutathione, Maltose Binding Protein (MBP) binds to surface-immobilized maltose or maltotriose, FLAG®peptide is recognized by a specific antibody, the enzyme O-6-alkylguanine-DNA alkyltransferase (known as SNAP-tag) binds to benzylguanine. The major drawbacks of all of them is the bulky steric hindrance that this fusion tag exert on the proteins, sometimes affecting their folding, stability, and activity.

- **Semisynthetic DNA-protein conjugates**, like DNA-Directed Immobilization (DDI) (51) of proteins, merge the high specificity of Watson-Crick base pair DNA recombination with the dynamic potential of protein interaction. Semi-syntheic ssDNA-Protein conjugates have been developed (51) and found extensive applications for self assembled protein layers. DNA micro and nanopatterning through self assembling was boosted for DNA microarray application in genomic and transcriptomic studies, and stable dense parrallel DNA micro and nanoarray can be produced routinely. Eventually, the use of different complementary ssDNA oligos tagged with different proteins of interest easily

transform a DNA micro array into a protein array, where the DNA sequence provides the address for the protein molecule on the surface.

- **Poly-histidine tags**, or His-tag, of 6 to 10 histidine residues (52, 53), was a fusion protein method originally developed for affinity chromatography of histidine-rich proteins. These are the most versatile example of fused peptides, so they merit a separate description. His-tag is of tiny dimension, rarely affect the folding and stability of the target protein since rarely produces destructive interaction with the fused polypeptide chain, and has a very low immunogenicity, so it doesn't —generally— affect antibody production from the recombinant protein.

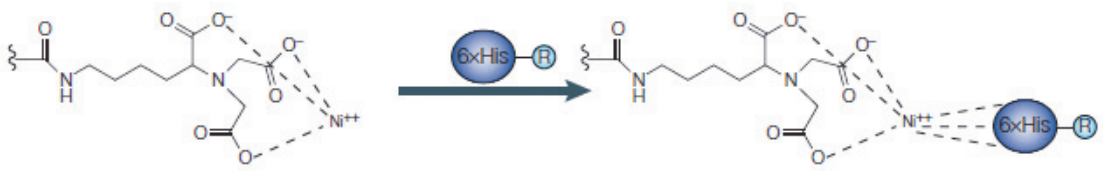

Figure 2.2: **NTA-Ni(II)-His-tag Immobilization Strategy** - Histidine coordination of a Ni (II) atom trapped on a surface is shown. Adapted from (46)

Complexation of histidine residues with immobilized transition metal ions offers powerful solutions. Transition metal ions such as Zn(II), Cu(II), Ni(II) in particular, or Co(II) are immobilized by chelating agents such nitrilotriacetic acid (NTA), thus maintaining 2 coordination sites free for histidines. This interaction can be very efficiently disrupted by competing coordinators such as imidazole, which selectively and rapidly remove the protein from the surface under mild conditions. Two are the major drawbacks: the long-term stability of the derivatized surface, that depends *in primis* on the density of NTA groups on the surface (53, 54), and the lack of simultaneous multiplexed functionalization, that is, each NTA group will react with whichever his-tagged protein is in the surrounding, so multiple proteins immobilization has to be achieved, if at all is possible, only in a sequential, non parallel, protocol, or has to be coupled with nanoscale dispensing of each protein that has to be immobilized.

Both DDI and NTA-Ni-His-tag system have been used in self assembled monolayer on gold and patterned with a variety of technique involving soft lithography and μCP as well as scanning probe lithographic technique like DPN and NG. Next chapters will review in much more details the achievements of the combination of these surface chemistry with AFM-based nanopatterning.

2.2.3 Nanostructuring the interface

Traditional microfabrication technologies like soft-lithographic techniques, microcontact printing (μCP), nanoimprint lithography (NIL), nanosphere lithography (NSL), electron beam lithography (EBL), focused ion-beam lithography (FIBL) are able to provide micro and nanostructured interfaces on which protein can be subsequently accomodated, either by physisorbtion, or secondarily to one of the many chemical surface functionalization already described[1]. Protein microarray were firstly fabricated with the use of an ink-jet printer based instrument, in which the ink was substituted by the protein solution. In spite of the high resolution nanofabrication techniques introduced, like EBL, FIBL, the concept remains very much similar: either the protein or a suitable chemical linker for it has be specifically confined to a target area. However, in addition to non nengligible costs of these equipments, and to the exquisite expertise required to operate them, two major issues still are not properly solved: compatibility with protein printing reagents and functionalization of the individual features with different proteins without compromising the entire surface.

Nanodispensing provides a mean for local delivery of the receptor molecule to its spot on the array with nanosized pipette; conductive atomic force microscopy (c-AFM)(56), dip-pen nanolithography (57, 58, 59), native protein nanolithography (60) as well as nanografting (61, 62, 63, 64, 65, 66, 67), have been successfully used for fabricating arrays of proteins with submicrometre resolution in native-like conditions. The advantage of Atomic Force Microscopy based lithographic technique will be addressed in details in the next chapter. The extraordinary versatility of this technique, that encompasses nanolithography, high resolution morphological

[1]Recent applications on protein immobilization have been extensively reviewed elsewhere. See for example (6, 44, 55)

studies, direct detection *via* interfacial proterties (simple topography, or molecular friction) of events taking place on surfaces, the possibility of coupling with electrical, electrochemical or optical detection methods, makes AFM the election methodology for *in situ* accurate investigation of biorecognition phenomena.

2.3 A small appendix on the sensitivity of nanostructured device

Characterization of binding events implies a carefully design of the assay that becomes crucial when nanostructured interfaces are used to present one of the binding partner.

2.3.1 A reminder for quantitative binding analysis

The biorecognition process between two interacting partner, a receptor[1] R and its ligand L can be described as a function of their concentrations:

$$[R] + [L] \underset{k_{off}}{\overset{k_{on}}{\rightleftharpoons}} [RL] \tag{2.1}$$

where k_{on} and k_{off} are, respectively, the association rate constant (in units of $M^{-1}min^{-}1$) and the dissociation rate constant (in units of $min^{-}1$).
Binding occurs when ligand and receptor collide due to diffusion with the proper collision energy and orientation; the association rate, that is, the number of binding events per unit of time is expressed as:

$$v(t)_{association} = [R] \cdot [L] \cdot k_{on} \tag{2.2}$$

Once binding has occurred, the ligand and receptor remain bound together for a random amount of time. The probability of dissociation is the same at every instant of time, i.e. it doesn't depend on the actual duration of the interaction. The rate of dissociation is:

$$v(t)_{dissociation} = [RL] \cdot k_{off} \tag{2.3}$$

[1]The term receptor is used here in a wider sense: it represents the protein in limiting and fixed amount in the assay, and usually —but not always— is the one immobilized in heterogeneous phase assays

At thermodynamic equilibrium, the forward and backward reaction's rate will balance each other, so that the net variation of the reactants and products is zero.

$$k_{on}[R] \cdot [L] = k_{off} \cdot [RL] \tag{2.4}$$

The law of mass action relates the relative concentration of the actors involved to the affinity constant:

$$K_d = \frac{k_{off}}{k_{on}} \tag{2.5}$$

The thermodynamic equilibrium constant, also called affinity or dissociation constant K_d, is a global descriptor of the binding behaviour at equilibrium condition, although only the knowledge of k_{on} and k_{off} may give insights on the molecular mechanism. The dimension of K_d is expressed in concentration units (M), and it point to the simplest interpretation of its meaning: at concentration of ligand L equal to K_d, the conentration of free receptor R equals the concentration of ligand bound receptor RL, that is, K_d equals the concentration of ligand necessary to achieve saturation of half of the receptor present in solution. It gives a measure of the affinity of the ligand for the receptor. The quantitative analysis of K_d, whether in solution or on surfaces, of protein-protein interaction governed by the law of mass action relies on the following specific assumptions:

- Interaction is reversible. In the simplest case, association is a bimolecular reaction, while dissociation is a unimolecular rection.
- All receptor molecules are equivalent and independent.
- Components do not undergo any chemical reaction and exist only in bound or free state.
- Interactions *are* measured at equilibrium.
- The measured response is proportional to the number of occupied receptor sites.

Provided that these assumptions are satisfied, the simple model of the law of mass action predicts the fractional receptor occupancy (the amount of receptors bound to ligand) at equilibrium as a function of ligand concentration. From an experimental

point of view, the relationship (at equilibrium) between ligand concentration and K_d has then to be re-arranged, and expressed in the form of free (f) or total (t) ligand and receptor concentrations:

$$K_d = \frac{[R_f][L_f]}{[RL]} \tag{2.6}$$

then, considering that:

$$[L_f] = [L_t] - [RL] \tag{2.7}$$

and that:

$$[R_f] = [R_t] - [RL] \tag{2.8}$$

the fractional occupancy, or fractional saturation of the receptor is:

$$\frac{[RL]}{[R_t]} = \frac{[L_f]}{K_d + [L_f]}. \tag{2.9}$$

Rarely surface-based assay can measure easily the amount of free ligand. Most of the experimental techniques, including the very sensitive ones, monitor binding through the evaluation of saturation of the receptors, with the underlying assumption that the signal retrieved is directly proportional to the amount of complex RL present at equilibrium. It is therefore useful to rearrange the relationship between bound and free ligand as follow:

$$[RL] = \frac{[R_t] + [L_f]}{K_d + [L_f]} \tag{2.10}$$

Unfortunately, most of the solid-surface experimental set up cannot afford at all the measurement of L_f. However, on the assumption that the depletion of ligand operated by the tiny amount of receptor immobilized on miniaturized devices is negligible, and since the L_t is the known variable, usually an approximate value of $L_f \sim L_t$ is used[1]:

$$S_{[RL]} = \frac{S_{max} + [L]}{K_d + [L]} \tag{2.12}$$

[1]Actually, if L_f is not explicitly measured an appropriate solution of the binding equation to obtain K_d requires that the quadratic equation relating fractional occupancy to L_t is solved:

$$\frac{[RL]}{[R_t]} = \frac{([R_t] + [L_t] + K_d) - \sqrt{([R_t] - [L_t] - K_d)^2 - 4[L_t][R_t]}}{2[R_t]} \tag{2.11}$$

where $S_{[RL]}$ is the measured signal proportional to bound ligand at a given $[L]$, and S_{max} is the measured signal at receptor saturation. In such a form, the dependence of $[RL]$ as a function of $[L]$ can be easily fitted to a rectangular hyperbola in order to derive K_d.
It is frequent to express the dependence of $[RL]$ on the logarithm of ligand concentration, so to obtain a sigmoidal dose-response curve of adsorption, which can expressed in varoius form, like:

$$S_{[RL]} = S_{L=0} \frac{S_{L=max} - S_{L=0}}{1 + 10^{LogK_d - [L]}} \tag{2.13}$$

2.3.2 Law of mass action and nanostructures.

When the experimental set-up involves the use of a surface, the previous description can apply only to idealized experiment in which the binding sites can be considered independent and freely accessible from the ligand partner (as it was already mentioned), and the concentration of the molecules on the surface should low enough that the binding reaction does not lead to significant depletion of the ligand molecules in the nearby solution, hence no concentration gradients is present, that is equivalent to assuming that the ligand has an infinitely fast diffusion constant. This is also known as "rapid mixing model" (31, 32, 34, 35, 38, 68). However, to enhance sensitivity, high density layer of immobilized probes are used, and some rough estimations on the possible performances of the device might prove useful. If a concentration gradient is present, the system become diffusion limited, and the performances of the device may be reduced, in terms of estimation of detection limits and K_d.

Introducing nano-scale device often increases the signal-to-noise ratio (S/N), an inherent advantage for signal transduction that would suggest a concomitant increase in the chances to detect very low amount of target analyte. However, if the target analyte is very diluted, the local concentration of capturing probes on the surface could be —in proportion— so high to deplete the analyte from the surrounding solution. Mass transport limitation, in this case, should be taken into account.

According to Sheean et al. [(35)] smaller patch size enhances the establishment of mass transport limits in the system. The authors examin theoretically the phenomenon, and suggest that reported femtomolar detection limits for bioassays are

likely to be an analyte transport limitation, not a signal transduction limitation. The consequence is that, without methods to actively direct biomolecules to a sensor, the nanodevice surface requires too much time to saturate with the target the functionalized patch at low concentration[1]. It has been reported (34) that for yes/no determination of target mass transport limit is not an issue, since device stability can reduce the incubation time to the minimum time required to immobilized the minimum numbers of molecules sufficient to give a detectable signal. However, quantification and binding characterization, that is our main concern, still depends on the average equilibration time. It has been widely examined (29, 31, 32, 69) that analyte preconcentration or active method (i.e. electrochemical gradients, magnetic nanoparticle driven concentration) to directly target the analyte on the spot are of moderate help if the physicochemical properties of the nanostructured interface are not well optimized.

The incubation time, for example, that is the time the system is allowed to reach equilibrium, needs to be chosen accordingly to the ligand receptor pair of the system. Let's take as a practical example recMoPrP(89-239) and either D18 or CloneP, the two recombinant, histidine tagged fragment of antibody that we used to selectively orient the prion protein on nanostructures, as it will be shown in Chapter 4. The incubation time was estimated from the kinetic parameters evaluated by Safar et al.[(70)] via Biacore experiment for the two antibody employed in our study: the average mean time $\frac{1}{k_{off}}$ of the complex is supposed to range between half and 19 hours, while the average lifetime ($ln2/k_{off}$) spans accordingly between half and 13 hours. However, considering the report of Kusnezow and coworkers [(32)], we may estimate in ideal condition (absence of mass transport phenomena and steric hindrance of binding site) that the ideal time as a function of target concentration $\frac{1}{k_{off}+k_{on}\cdot[target]}$ for signal "development", that is the approaching of the thermodynamic equilibrium, is shorter: from 4 second at a recMoPrP concentration of 900nM, to 12 minutes at 300 nM, 1 hour at 3nM and 5.6 hours at 95 pM concentration. In our experiment, we doubled the theoretical incubation time while performing the experiment to take into account eventual deviation from ideality (ee Chapter 4).

[1]Deriving a simple but useful steady state accumulation equation $Accumulation(t) = 4D \cdot (N_A \cdot C_0) \cdot t$, the average time is estimated to be of tens of hours at fM concentration for a 1 μm^2 patch

Heterogeneous phase microarray are modelled as two compartment model system,(32, 35) since the presence of a solid phase support affect the diffusion constraints of an ideal bimolecular reaction in solution. If initially the reaction is governed by the kinetic rate constant of the specific macromolecular pair involved, then it becomes progressively limited by the diffusion rate of the target analyte from the bulk solution to the reaction spot. Even in the steady state condition, the prolongation of the estimation time actually is not dramatic, due to the small patch size compared to standard microarray systems (31). Assuming the receptor molecule as a square of 4×4 nm^2, and therefore that the density of receptor ρ on a 1x1μm2 patch is 10^{-11}moles $\cdot$ cm^{-2}, and assuming a slow diffusion coefficient for the recMoPrP of $10^{-10}cm^2s^{-1}$, the Damkoehler number can be roughly estimated ($\rho \cdot \pi \cdot R \cdot k_{on}/4D$for a circular spot (31)) and used to correct with a proportional factor the ideal time (the time needed to reach the steady state between the bulk solution and the compartment surrounding our patch, that is in our case negligible). The reaction duration actually benefit of the small size of the patches we chose to fabricate: they are small enough not to deplete significantly the target analyte in the reaction site. However, if higher affinity constant antibodies were used, that would have terribly affected the performance of the assay: an increase in affinity of 2 orders of magnitude (let's say, in the 20 pM range), usually related to an equivalent increase in the off rate reaction constant, k_{off}, can actually rise the ideal reaction time to more than 60 hours at pM analyte concentration without any stirring or analyte concentration device. Concerning prion detection, methods like PMCA (protein Misfolding Cyclic Amplification) or enhanced concentration/precipitation with polyoxometalates will surely improve the analytical performance of our device.

3

Manipulating and Measuring Biomolecules with Atomic Force Microscopy

This chapter will detail how Atomic Force Microscopy is used to fabricate and characterize nanopatterns of biomolecules. Before that, there we will overview few fundamental concepts about the Atomic Force Microscope that are instrumental to the description of nanografting, the AFM-based nanolithographic technique that allowed us to orient, among others, the prion protein on nano-scaled structures.

3.1 Atomic Force Microscopy

Atomic Force Microscopy (AFM) belongs to the family of scanning probe techniques (SPM) , which rely on mechanically scanning a sharp probe to investigate surface properties with extreme spatial resolution. After the invention, in 1981 with Roehrer, of Scanning Tunneling Microscopy (STM), a technique based on the phenomenon of a tunneling current between a metal needle and a conducting sample, Gerard Binnig had the intuition that surfaces could be imaged by using a force, and in 1986 Binnig, Quate and Gerber reported the first use of the Atomic Force Microscopy (71). In particular, this was made possible by attaching a sharp tip probe to a cantilever, which deflection could be sensed with angstrom resolution. Scanning probe microscopies can be classified on the basis of the different nature of the probe

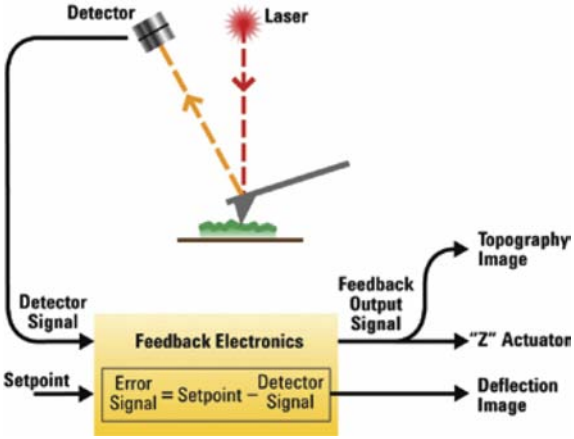

Figure 3.1: **Schematic diagram of Atomic Force Microscopy** - Adapted form "The AFM Almanac", Agilent Technology.

tip-sample interactions exploited for imaging (electrical, like STM, mechanical, such as AFM, optical, or a combination of these, like SNOM, Scanning Near-field Optical Microscopy), nonetheless, all scanning probe techniques share common features:

- A sharp probe tip (usually the tip radius of curvature is about 10 nm for standard probes) attached to a soft microsized cantilever spring (whose spring constant varies, depending on the applications, from the tens of pN/nm to a few tens of nN/nm).
- A way of sensing the cantilever deflection, usually a beam-deflection optical detection scheme, in which a diode laser beam is reflected from a mirror-like cantilever; the position of the reflected beam is sensed with a (four element) position sensitive photodiode.
- A feedback system, that is able to monitor and control the cantilever deflection associated with the variation of a monitored parameter sensitive to the tip-sample interaction, parameter that is usually kept constant with reference to a set value (as schematically depicted in figure 3.1.
- A mechanical scanning system, based on piezoelectric elements, which allows for accurate relative movement of sample and tip in a raster manner, in the x-y plane (lateral resolution), and a Z-actuator, composed of piezoelectric material as well, to act on the vertical relative movement of the tip.

Atomic Force Microscopy operational modes are usually distinguished on the basis of the force involved in tip-sample interactions, the time-scales involved in the interaction (that influences the time the tip is in contact with the surface), and the proximity of the sample to the probe tip. All modes enables the user to collect accurate topographic images of substrates with nanometer lateral resolution, and, depending on the operational mode, additional information on interfacial properties.

3.1.1 Contact Mode - AFM

In Contact Mode (CM) AFM, sometimes referred to as static mode AFM, the tip is kept in constant contact with the surface, and the interaction is dominated by relative short range forces. In idealized conditions (e.g. in ultrahigh vacuum) when the cantilever tip approaches the sample surface, long-range van der Waals forces start acting upon it (these forces are sensed at the distance of a few tens of angstroms). Then when the tip gets nearer to the surface (some angstroms) repulsive force starts predominating. The force exerted on the tip by the surface causes bending of the cantilever beam. By measuring the cantilever deflection from its equilibrium (non interacting) position, it is possible to evaluate the tip-surface interactive force (that is qualitatively described by a Lennard-Jones potential curve).

The signal from the photodiode detector is the (almost) vertical deflection of the AFM cantilever (deflection signal), measured usually at or near the free end of the cantilever using a reflected laser beam. The *error signal* is the difference between the deflection signal and the AFM feedback system's setpoint value, and it is used by the feedback system to keep the interaction with the surface constant (see figure 3.1). In other words, the user choose a minimum interacting force for imaging purposes. As the tip scans the sample, variation in the topographic profiles may cause this interaction to change: the error signal registered is used as a feedback signal to drive a z-actuator that either lift up or down the tip relative to the sample, so to correct a too strong or a too weak (respectively) interaction, with reference to the set point. In this way, a topographic profile is reconstructed.

CM-AFM enables high lateral resolution —that can achieve in some conditions atomic and molecular resolution— although tip deterioration, shear stress and sample damage are common experimental failure encountered in the practice. Measure-

ments can be performed both in ambient air or in liquid environment, on a variety of specimen, including those of biological interest. In the latter case, the interaction force (the set point) is usually kept to a minimum, not above 1 nN, in order to maintain the integrity of soft biological materials, like DNA or protein deposited on bare mica, nanopatterned biomolecule, and living cells (72).

3.1.2 Lateral Force Microscopy

Lateral Force Microscopy (LFM) is a derivative imaging technique of CM-AFM monitor the lateral deflection (cf. vertical deflection in standard contact mode) of the cantilever while the tip fast scan direction is perpendicular to the AFM cantilever's long axis. As a result, the detector collects also a non negligible lateral defection signal from the cantilever's twisting motion as the raster scanning proceeds. The strength of the lateral deflection signal is related to the friction force between the sample surface and the tip. This is why LFM is also called Friction Force Microscopy. However, the friction signal is highly susceptible to topography variations; geometrical contribution from roughness, or patterns, adds topography convolution to the lateral signal. In order to separate the variation in friction force from the geometric contribution, two lateral force signal are recorded (a forward and backward trace during each round-trip cycle of the raster scan). Then the difference between the two signal is the net friction force image. Friction signal are very sensitive to variation in the chemical properties of the sample, that influences the proximity interactions with the tip, and give additional information on material properties.

3.1.3 Non Contact Mode - AFM

In Non Contact mode (NC-AFM), the AFM cantilever is driven to oscillate near its resonance frequency (73). The cantilever is kept away from the sample surface (within few tens of nanometers) were long range forces (electrostatic, magnetic, attractive van der Waals forces) are predominant and accessible to the operator. The oscillations are such that the free end of the cantilever and the tip move along a gently curved trajectory on a plane perpendicular to the XY plane. The amplitude, the resonance frequency and the phase shift of the oscillation are the monitored

parameters that are influenced and link the dynamics of a vibrating tip to the tip-surface interactions.
In Amplitude Modulation (AM) AFM , also known as Intermittent Contact Mode or Tapping Mode®, the observable that the feedback system controls is the cantilever's oscillation amplitude. The measured amplitude is compared with a setpoint value, and the difference, the error signal, is the input into the feedback system (as the error in the deflection was in CM-AFM), the output of which drives the Z-actuator that controls tip movement. Since the oscillation amplitude is influenced by the long range forces exerted by the sample on the tip, amplitude as a feedback parameter is used to reconstruct the topography of the sample surface. Additionally, complementary information on material properties variations on heterogeneous surfaces could be mapped by recording the phase shift between the driving force (the input signal that triggers the cantilever's oscillation) and the actual tip oscillation.

One of the main advantages of AM-AFM over CM-AFM is that, since the tip only intermittently touches the sample surface, lateral shear forces that may alter the tip or rearrange (i.e. damage) the sample surface during scanning are significantly reduced. Despite the difficulties of operating AM-AFM in liquid environment (where oscillation frequencies are dumped significantly by the viscosity of the aqueous medium), it has been successfully applied to high resolution imaging of model membranes, membrane proteins, DNA-protein complexes, amyloid fibrils (11), protein nanopatterns and living cells, like neurons (74).

3.2 Nanopatterning Biomolecules with Atomic Force Microscopy

AFM based nanolithographic techniques have been already mentioned as very versatile methodologies for a highly controllable manipulation of matter at the nanoscale. First attempts of modifying surfaces with SPM date back to 1990 when Eigler and coworkers (75) reported the use of STM in ultra high vacuum to slide single Xenon atoms to compose the IBM logo.

With the advent of AFM, matter manipulation at the nanoscale was not anymore confined to low temperature, high ultra vacuum environments, and a few years

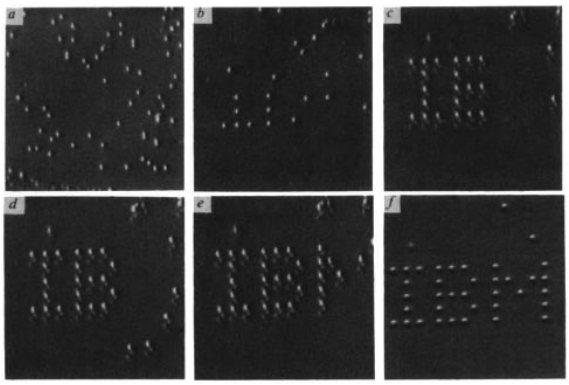

Figure 3.2: **Single Xenon Atom Manipulation with STM** - Construction of IBM logo manipulating step-by-step single Xe atoms on Ni surfaces. Adapted from (75).

later the two major widespread AFM based lithographic techniques were introduced, namely nanografting (76), 1997, and Dip Pen Nanolithography (59), 1999. Even localized tip induced *in situ* chemical reaction can be performed, using conductive tip AFM to induce electro-oxidation on the substrate, like, for example, nanoelectrochemical patterning, in which the tip is used to convert electrochemically the head group of a monolayer into another functional group. This technique however cannot be performed in liquid and is not therefore suitable for successful immobilization of protein in native-like conditions.

3.2.1 Dip Pen Nanolithography

The invention of Dip-Pen Nanolithography (DPN) dates back to 1999 (59). Conceptually, it isn't very much different from μCP, or molecular stamping, but makes good use of the high lateral resolution of AFM combined with the self assembly capability of molecules like alkylsilane on silicon oxide, and thiols on gold. It is a nanoscale top down approach to delivery, coupled to a bottom up approach to spontaneous molecular organization. It is a scanning-probe based patterning technique in which molecules could be directly transported repeatedly from a molecule-coated tip (previously dipped in an "ink" reservoir) to a surface in an additive manner, as shown in figure 3.3. Molecules that serve as inks are coated on an AFM tip and

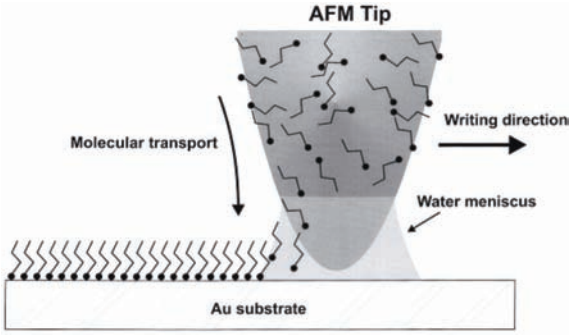

Figure 3.3: **Cartoon of Dip Pen Nanolithography technique** - A tip, previously dipped in a solution of a thiolated molecule, is scanned over the surface to deliver molecule at specific location. The size meniscus of the meniscus influences the thiols tranfer to the surface, and therefore has to be carefully controlled through a humidity chamber. Adapted from (59).

transported to the surface by engaging the tip and scanning. Inks that chemisorb specifically and self assembly on the surface are preferred to generic physisorbing molecules. The patterns are produced in a binary one-to-many array configuration (one molecule, many spots) with physical architectural parameters controlled by the movement of the AFM tip. DPN utilizes the water meniscus that naturally forms at the point-of-contact between tip and surface to help control ink transport, and therefore requires a humidity-controlled chamber to regulate ink transport. The remainder of the surface is then passivated to prevent non specific binding in subsequent uses of the nano array. The introduction of multiple cantilevers array boosted the application of DPN for the simultaneous fabrication of highly dense parallel array of molecules, in which patterns feature size of about 100 nm $\times$ 100 nm (58). Then, with the introduction of hollow cantilevers arrays, in which the tip is actually a sort of nanopipette dispenser, multiple proteins can be patterned in haglhy dense array for subsequent high-throughput applications.

It has been argued that (57) DPN is the only AFM-based nanolithography that is actually based on the delivery of molecules on the surface without any simultaneous delivery of energy, and that this makes DPN the only constructive (as opposed to destructive) technique. DPN, like all bottom up approach, exploits the self assembling properties matter, hence supplying energy to the molecules is not necessary for the assembly to happen. However, introducing energy into the system opens alternative

self-assembly pathways, that can lead to facilitate route of spontaneous organization of the desired molecules. If the energy delivery is accompanied by the introduction of appropriate additional boundary conditions, like physical confinement, the spontaneous organization in self assembled pattern can be not only enhanced but also modulated and controlled actively. This is what nanografting does.

3.2.2 Nanografting

Nanografting was reported in 1997 by Liu and coworkers (76). It is an AFM nanolithographic based techniques combined with the surface chemistry of thiol adsorption on gold surfaces, with a ten better resolution than the much more widespread DPN. The procedure of nanografting is relatively simple. Starting from imaging (under a small force) an alkanethiol SAM in a liquid medium containing a different kind of thiol that has to be patterned, by scanning at increased loading force, the tip catalyses the substitution of the existing monolayer and favours the self assembly of the new molecules in the chosen area (cf. Figure 3.4, panel a). The accelerated chemisorption rate is attributed to a change in the pathway for the self-assembly process. The spatial confinement makes it geometrically more probable and energetically more favorable for the initially adsorbed thiols to adopt a standing-up configuration directly in this microenvironment. It has been shown by SPM and diffraction studies that spontaneous self assembly of thiols onto gold surfaces in an unconstrained environment involves a two step phase. Initially, molecules attach to the gold with the chains parallel to the surface, a reaction intermediate known as the lying-down phase; then, as a result of collisions and lateral pressure, thiols pack in a standing up phase with a tilt of 30° to the surface normal. (64, 77)

Nanografting is thought to alter the initial Langmuir (or modified Langmuir) kinetic pathway of molecule adsorption (77), basically lowering the activation energy for the spatially confined self-assembly process. While scanning at high loading force, the tip creates a transient reaction environment in which the newly exposed gold surface is spatially confined by the surrounding thiols and the tip. The adsorbing thiols, present at high local concentration compared to that of the desorbing ones, are restricted in a confined area so that the “laying-down phase” is skipped

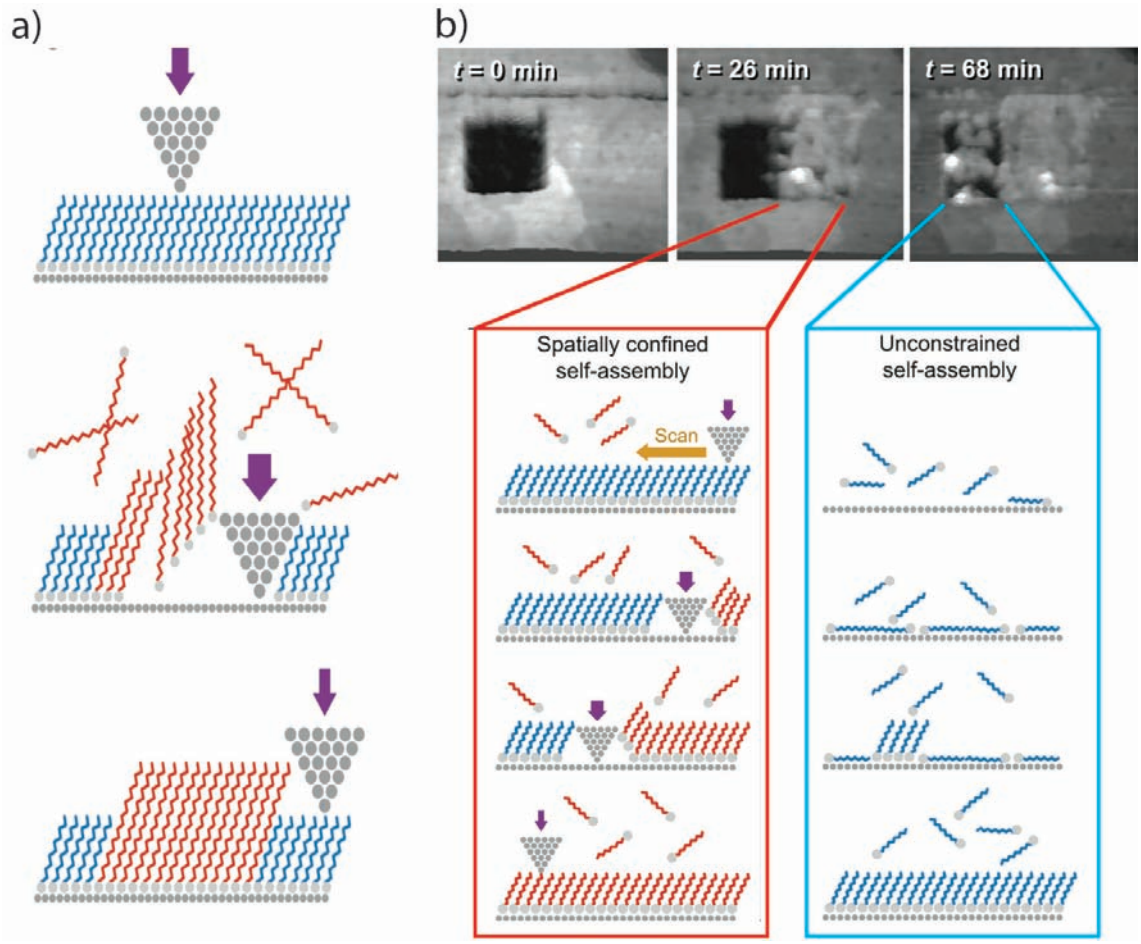

Figure 3.4: **Cartoon of Nanografting technique** - a) Nanografting process. b) topographic images of C18 self assembly on gold, as a function of time and of the surface reaction pathway. After a portion of the surface is shaved (i.e. bare gold is exposed), a solution of C18 molecule is incontact with the sample. Self assembly in spatially confined process like nanografting is much faster than the spontaneous self assembly in unconstrained condition. Adapted from (64).

and thiols readily adopt the "standing up" configuration. The standing-up configuration facilitates the chemisorption of sulfur to gold and the packing of the chains to form the SAM, and it is also enthalpically favorable because the interactions between the newly adsorbed molecules and the surrounding thiols help stabilizing the transition states for the self-assembly process. It has also been shown by SPM that the order and packing of the nanoassembled monolayer is considerably higher than in unconstrained SAM adsorption.

This nanolithographic technique has been chosen for tunable surface nanopatterning of a variety of molecules, including alkanethiols as internal reference for accurate measurements of electronic properties of molecular junctions (78), DNA oligonucleotides for surface hybridization studies (63) and protein interaction studies (66), and a variety of suitable linker for protein immobilization that will be addressed in the next section (61, 62, 65, 67, 79, 80). Many variants of nanografting have been proposed, and are referred to as **reversal nanografting**, when the inert molecule is patterned into a SAM of desired surface functionalization, and **tapping mode nanografting**, when patterning is achieved not in CM-AFM as usual, but in AM-AFM with strong intermittent interaction between the tip and the sample.

3.2.3 Native Protein Nanolithography

Native Protein Nanolithography has been introduced in 2008 by Tinazli et al (60). It can be described as an "erasing technique": a SAM, already functionalized with a protein of interest, is then scanned in a particular variant of the AM-AFM mode, a second vibrational AFM mode that was named as contact oscillation mode. Immobilized proteins are detached by the tip and replaced by other proteins, which are selectively self-assembled from the bulk. The technique relies upon selective removal at specific location of a "protecting protein" and on the self assembly of desired his-tagged proteins on a SAM presenting Ni(II)-loaded NTA functional groups, and in principle can be applied to any SAM derivitized with proteins (or other macromolecules) *via* affinity capture system.

3.3 Nanografting as a tool for protein immobilization

Technically, nanografting is performed in a closed liquid cell were the substrate carrying the hosting SAM is mounted. The cell is filled up with a solution of the thiolated molecule that has to be patterned. Since the hosting SAM is usually made of alkylthiols, not so prone to water solubility, ethanol, 2-butanol, or an aqueous solution containing a certain percentage of ethanol or trifluoroethanol (TFE) has to be employed. Small percentages of organic solvent can be tolerated by many proteins (but not all); among them, TFE is well known and widely used because it promotes intramolecular hydrogen bonding formation to the detriment of solvent (water) - protein interactions: α-helix secondary structure is, for this reason, promoted and stabilized by TFE addition. In some occasion, reducing reagent like TCEP(tris(2-carboxyethyl)phosphine) can be added to maintain thiol groups in the reduced state. Unlike DTT or mecaptoethanol, TCEP is not involved in the exchange reactions with self-assembled mono- layers (SAMs) of thiols.

SAM are firstly imaged in liquid at low load to select the area where to fabricate the nanostructures. The desired patches are usually obtained within the SAM by scanning the AFM tip at considerable loading force (above a threshold of, let's say, 70 nN) in a confined area of desired size. In this way the alkylthiol SAM phase is exchanged with the thiolated linker or protein. The rate at which the tip is scanned over the selected area may influence the process especially if bulky molecules are involved. With nanografting, molecule's packing density can be routinely varied in a reproducible manner by operating on two parameters: primarily by varying the concentration of the grafting solution, and secondarily by changing the ratio between the actual area scanned by the tip and the area of confinement (scan density ratio, as schematichally drawn in figure 3.5. Tuning these multiple parameters, even in the same experimental run, allows the user to tailor the fabrication technique to the particular molecule to be pattern. Moreover, the use of a hosting SAM with "bioresistant" properties (i.e. oligoethylenglycole terminated SAM) provides an inert internal reference, that allows for intrinsic differential measurements of interfacial properties on the nanostructures.

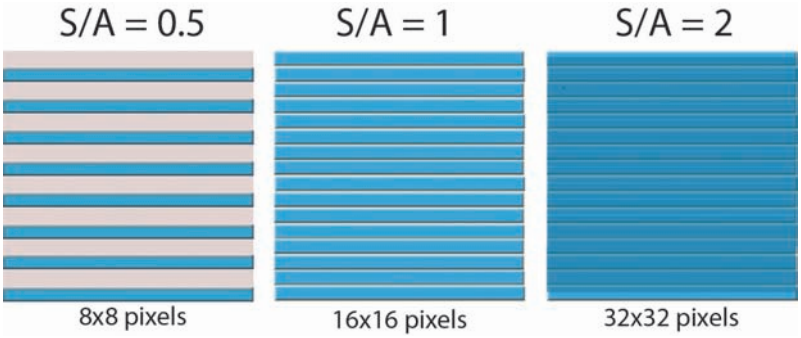

Figure 3.5: **Surface density moculation *via* Nanografting** - Molecule's packing density tuned by changing the scan density ration $R_{tip} \cdot lines/area$, that is the ratio between the actual area scanned by the tip and the area of confinement. A visual cartoon is depicted in the specific case of a tip/surface contact area diameter of 10 nm, image size of 160×160 nm^2, and the number of line wrote by the tip on the fast scanning direction (pixels) indicated in the three cases.

3.3.1 Probing lateral heterogeneity of protein structures with nanografting

Liu and coworkers reported recently (67) the use of nanografting and reversal nanografting to study the effect of size and distribution of functionalized nanoscale spot (as little as 25 nm^2) on subsequent protein immobilization. Strong dependence on the dimension and spatial distribution of protein binding sites within arrayed pattern were investigated in antibody recognition, covalent attachment via primary amine residues and surface-bound aldehyde group. The coverage as well as the orientation of protein molecules was regulated, to a large degree, by changing the dimension and separation of each nanoelement, in the case of biotin and antibiotin IgG reactions over biotin nanopattern, and by changing the nanografting conditions, in the case of covalent immobilizations of IgG and Lisozyme on aldehyde terminated thiols. The study dealt mainly with the AFM study of the later heterogeneity and protein distribution after immobilization on these nanostructured interfaces, but it was not investigating how these interfacial properties were influencing the stability and functionalities of those proteins.

3.3.2 Direct Nanografting of Cysteine-tagged protein

Direct linking of proteins to a gold surface is provided with the introduction of an extra (or multiple) cysteine at the N- or, more often, C-terminal of the protein. The proximity of the gold surface poses some concerns about the folding stability of the polypeptide to be immobilized, so initial experiments were performed on *de novo* combinatorial peptides of know stable folding (79, 80), and later on, native protein nanografting was achieved with recombinant Maltose Binding Proteins (61).

***de novo* three-helix bundle peptides** can be chemically synthesized from well established computational design of motifs such as coiled coils. Such systems can be selectively assembled by appropriate choice of hydrophobic core residues. For example, a repeat of the hydrophobic amino acids leucine (L) and valine (V) at the first and fourth positions of a heptad of amino acids has been reported to confer trimeric specificity (80). For peptides shorter than 30 amino acids, however, such specificity may not be as marked, so Case et. al. chose a design that exploited the coordination requirements of transition metal ion in order to dictate the topology of the resulting threepeptide ensemble. A 78 amino acid iron(II) complex [Fe($R_pV_aL_d$-C26)$_3$] was nanografted into a C18 alkanethiol monolayer previously assembled on a Au(111) surface and characterized by AFM.

Specifically, each peptide had a bidentate 2,2'-5-carboxy-bipyridyl ligand appended covalently *via* an amide linkage to the N terminus. Addition of ferrous ion sequesters the three peptide ligands to form the octahedral $[Fe(bpy)_3]^{2+}$ complex, thus increasing the effective local peptide concentration. The ensuing hydrophobic collapse of the interior of the structure is accompanied by folding of the tertiary parallel three-helix bundle protein architecture. The folded structure is designed to present the C-termini of the three helices to an appropriate surface in a tripodal manner, where, to enable the necessary chemisorption on gold, the helices were terminated with D-cysteine residues. D-cysteine is a "non natural" aminoacid (the one biosynthesized by living organism is L-cysteine), but was choosen because the unnatural D- stereochemistry presents the thiols coaxially with the helices rather than equatorially, which would be the case were L-cysteine to be employed. The nanopatterns were then imaged at low forces to ensure the effective immobilization

via height (topographic) measurements. Differential height measurements with reference to the hosting C18 SAM gave an average value of the height difference is 3.1 nm, implying a measured height for the proteins of 5.3 nm,in very good agreement with the 5.2 nm size extrapolated from molecular model. Increasing loading forces showed that these peptide nanostructures of 100 nm × 100 nm are resistant to mechanical load up to 15 nN; then they become damaged.

Interestingly, experiments were also attempted using the truncated 19-residue analogue $[Fe(R_pV_aL_d\text{- C19})_3]^{2+}$, however, the patterning showed a broad distribution of low heights (0.8 nm). It is likely that the hydrophobic gold surface promotes unfolding the three-helix bundle upon contact, and the additional 900 cal×M^{-1} stability conferred by the additional two turns per helix in $[Fe(R_pV_aL_d\text{- C26})_3]^{2+}$ is necessary to overcome this thermodynamically driven unfolding.

***De novo* helix bundle combinatorial proteins** were nanografted and characterized onto the (111) surface of gold (79). The particular protein used in this second study on synthetic proteins was recombinant engineered to contain a Gly-Gly-Cys linker at its C-terminus,[1] and the protein was named S-284-C, since it is based on the previously characterized S-824 *de novo* protein. S-824 was chosen from a"binary cod" strategy library of 102-residue sequences designed to fold into 4-helix bundles. The 3D structure of S-824 was determined by NMR, and as specified by the binary code design, it is a 4-helix bundle with a polar exterior and a hydrophobic core.

Compared to the previous case, Hu and coworkers reported that nanografting this bulky protein (compared to the sinthetic peptide) was a very delicate process. The average height of the grafted protein patterns was found to be somewhat higher than expected from the known NMR structure of the protein: measured heights placed the top surface of the protein approximately 5-8 nm above the gold surface, whereas the expected height would have been 5.5-5.8 nm above the gold surface. The entire protein (MW > 12 KDa) was bound to the gold surface by a single thiol linker at the C-terminus of the protein, with a much smaller cross-section than the 4-helix bundle protein. Therefore, if all the sulfhydryl groups in the solution seek the

[1]Please note that the protein was produced *via* recombinant DNA techniques, that is, bacterial cells were forced to produce the protein from a properly transfected DNA sequence. Therefore, the cysteine introduced as a tag is a L-cysteine, the natural enantiomer

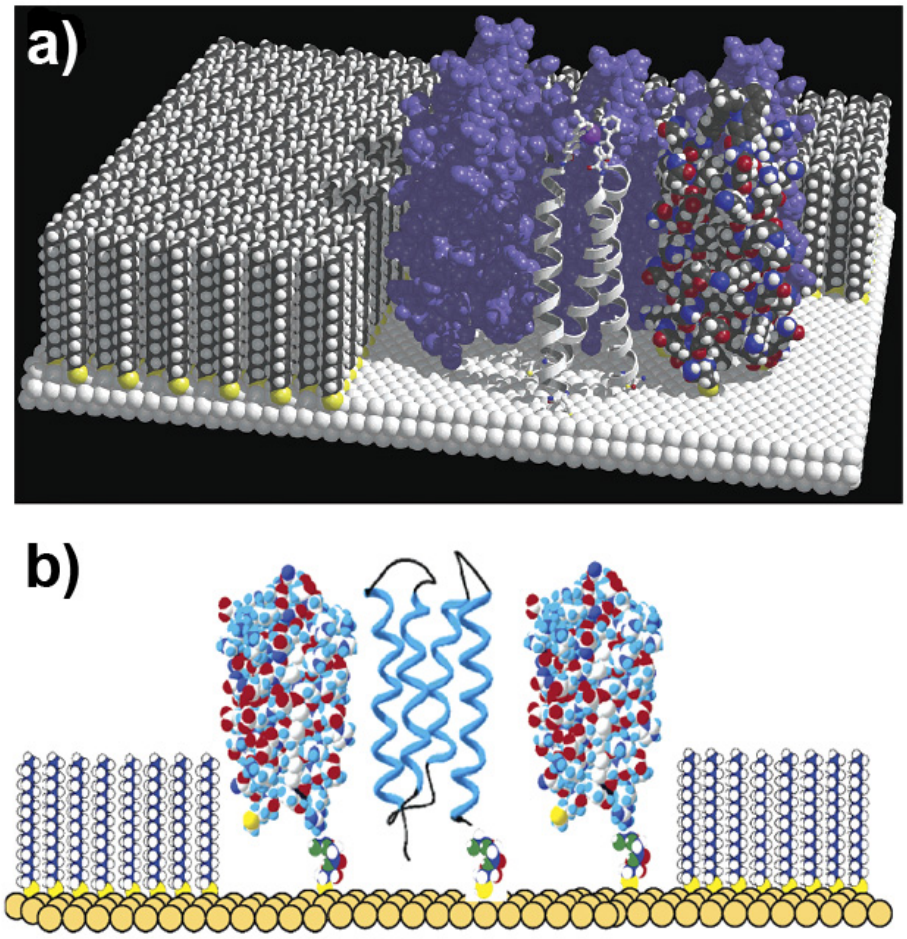

Figure 3.6: **Direct Nanografting of *de novo* polypeptides** - Cartoon depicting stable polypeptide immobilization through nanografting of (top) [Fe($R_pV_aL_d$-C26)$_3$]$^{2+}$, and (bottom) combinatorial protein S-284-C. Adapted from (79, 80).

gold surface, then there would not be sufficient space for the 4-helix bundle proteins to pack, a situation that Hu and coll. depict as "packing mushrooms": if the vertical stems achieve close packing at their bases, then close packing will not be possible for the mushroom caps. This effect might destabilize the formation of 4-helix bundles in the nanografted patches and favour protein refolding upon adsorption to the gold substrate, thereby producing a long 2-helix hairpin.

Compression of the nanografted patches by an external force (below 10 nN) was reversible but showed some hysteresis. Interestingly, both the energy required to deform the immobilized protein patterns and the energy defined by the hysteresis loop were found to be of the same order (43 kcal/mol) as the energy required to unfold the monomeric protein in solution, putting the basis for measuring the energy stored in proteins by mechanical compression as a method for probing the structural stability of proteins packed at high density.

Maltose Binding Protein (MBP), engineered with a C-terminal double cysteine tag, was effectively nanografted by Staii et al onto EG_3 (triethyleneglycole) terminated SAM grown on gold (111) surface in native conformation, and *in situ* bioactivity of these proteins within the fabricated nanopatterns was assessed through lateral force measurements, as illustrated in figure 3.7. Protein ligand-binding function was maintained upon the immobilization process and was not affected by the addition of the cysteine dipeptide, the spatial confinement associated with nanografting, and the interaction between the protein and the Au substrate.

Maltose Binding Protein belongs to the superfamily of the Periplasmic Binding Proteins, involved in bacterial chemotaxis and uptake of nutrients in the surrounding environment. MBP has a binding domain able to recognize sugars like maltose and maltotriose. Upon binding, the ligand (e.g. maltose or maltotriose) is buried into the the binding cleft, and the protein undergoes a conformational transition. However, the contribution in height is negligible, so the binding events had to be detected through friction measurements. The maltose (or maltotriose) mediated conformational changes within the MBP have been found to change the AFM-tip-protein interaction, therefore causing the frictional signal to change. The authors studied the change in the frictional force above the protein nanopatterns as a function

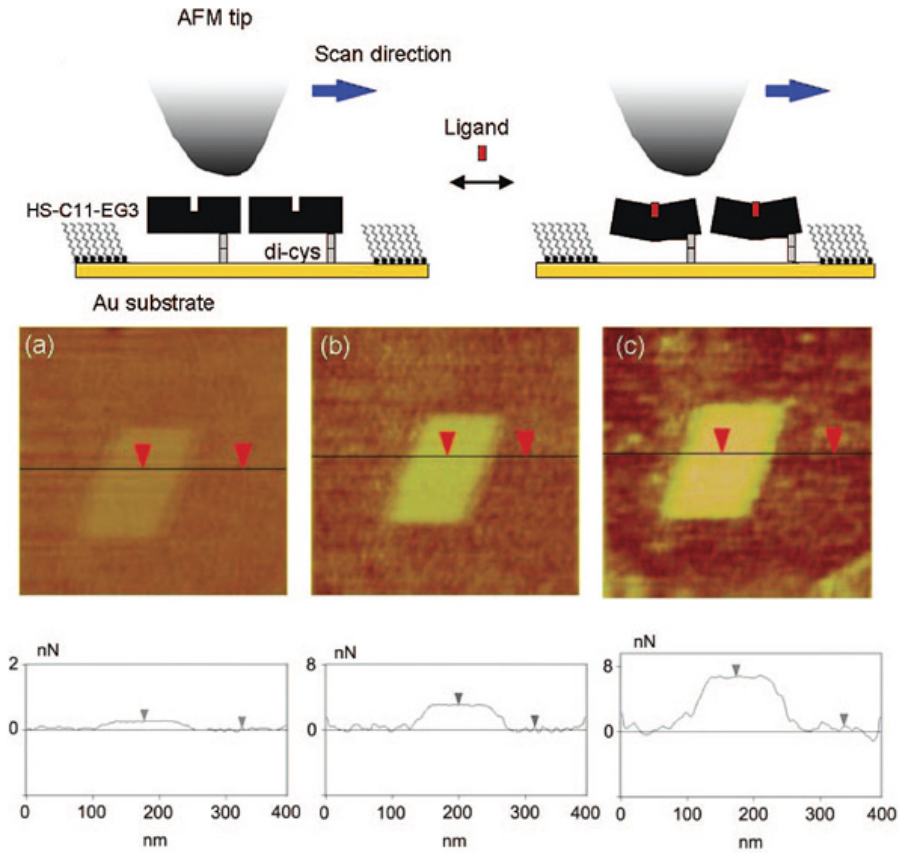

Figure 3.7: **Direct nanografting of MBP in native conformation** - MBP-Cys_2 was nanografted efficiently in stable conformation. Biochemical activity (maltose or maltotriose binding) was ascertained through friction force measurements: the normalized friction force (as compared to the surface) was proportional to MBP saturation. Adapted from (61, 65).

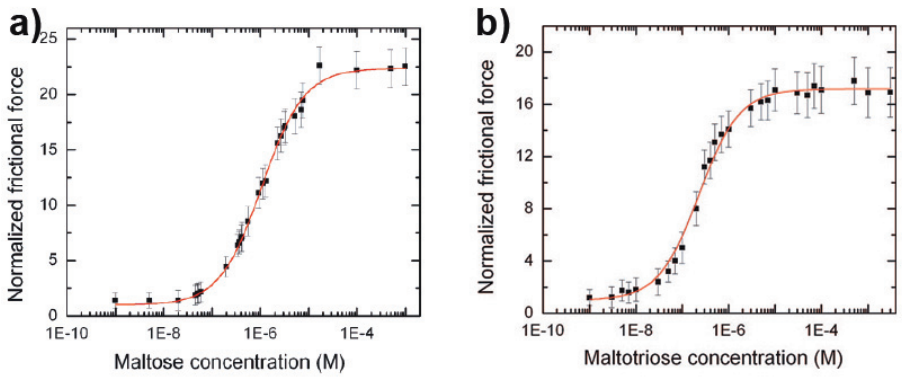

Figure 3.8: **Friction Force based binding tudies.** - Sigmoidal dose-response curve of normalized friction force as a function of ligand concentration allows for accurate estimation of binding parameters apparent dissociation constant for the MBP-cys-cys/maltose system to be $K_{dmaltose} = (1 \pm 0.04)\mu$M, and $K_{dmaltotriose} = (0.22 \pm 0.01)\mu$M for the maltotriose ligand. Adapted from (61, 65).

of maltose or maltotriose concentration, and they determined apparent dissociation constant for the MBP-cys-cys/maltose system to be $K_{dmaltose} = (1 \pm 0.04)\mu$M, and $K_{dmaltotriose} = (0.22 \pm 0.01)\mu$M for the maltotriose ligand, which is close to the value of 0.16 μM reported in the literature for proteins in solution using both fluorescence and rapid-kinetic techniques. The particular orientation of the nanografted MBP-Cys_2, which exposes the binding sites to the buffer solution, facilitates the the accessibility of ligand binding sites without impinging on the determination of apparent binding affinities.

3.3.3 Nanografting of DNA as a tool for DNA directed protein immobilization on nanoarrays

Nanografting of thiolated oligonucleotides is a well-established techniques, that aimed at the very beginning at the understanding how spatial confinement in localized spot on an array affects the performance of the devices, especially referring to hybridization of complementary target sequences. ss-DNA oligonucleotides (between 15 and 60 bases) functionalized with a $HS-(CH_2)_6-$ linker at the 5' [1], are nanografted onto EG_3-SAM grown on templated stripped gold, in a mixture

[1] depending on the application, a 3' modification can be introduced

of buffer and ethanol (with ethanol usually not exceeding 50 %). SENIL laboratory has developed a solid expertise in the controlled immobilization of thiolated DNA probes *via* nanografting (62, 63, 66) and how the ordered packing of probes within the nanografted patch allows for the exploration of hybridization pathways otherwise not accessible to the conventional DNA SAM. In fact, nanografted DNA structures allowed for hybridization efficiency considerable higher than those reported on conventional self assembled surfaces. The hybridization efficiency was effectively probed with topographic measurements and with the investigation of the viscoelasticity properties of ss-DNA and ds-DNA nanostructures as a function of an applied external force, even in direct comparison with adjacent unconstrained SAM of the same DNA (63). These DNA nanostructures have been used also to investigate the effect that the steric hindrance introduced by surface bound DNA nanostructures have restriction enzyme reactions (66).

Interestingly, ss-DNA nanoarrays can be easily transformed into protein nanoar-

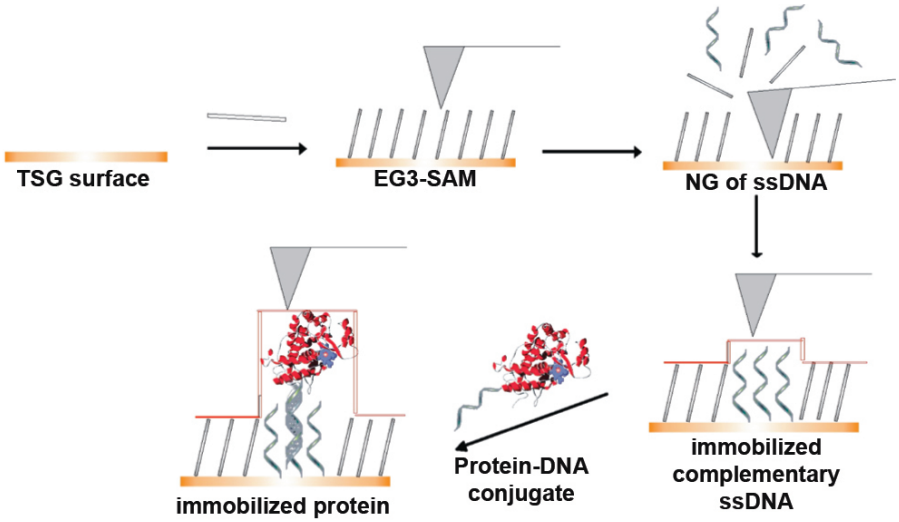

Figure 3.9: **Cartoon of DDI protein immobilization on nanografted DNA-arrays** - Complementary thiolated ssDNA is nanografted into an EG_3 SAM. The protein of interested, chemically linked to ss-DNA, is then immobilized specifically through base pair recognition. AFM topographic profiles are used to assess protein immobilization on the surface. Adapted from (62).

ray if the surface is hybridized with a complementary oligonucleotide strand conjugated the protein of interest, as shown in figure 3.9 (62). Then, biorecognition

events can be detected by topographic measurements (a label free approach) even in complex matrices. The combination of nanoscale parallel fabrication of multiple sequence array with the DNA Directed Immobilization (DDI) of proteins has been proven able to immobilize specifically different proteins in an array configuration in active conformation, to recognize the cognate antibody without loss of affinity, and to detect selectively the same specific antibody even in a complex matrix like standardized human serum. In the latter case, a patch array of three different ssDNA sequences was fabricated, in order to produce a negative control spot, a spot for DDI immobilization of streptavidin (STV), and a third spot for DDI immobilization of glucose oxidase (GOx). The two DNA-protein conjugates hybridize specifically

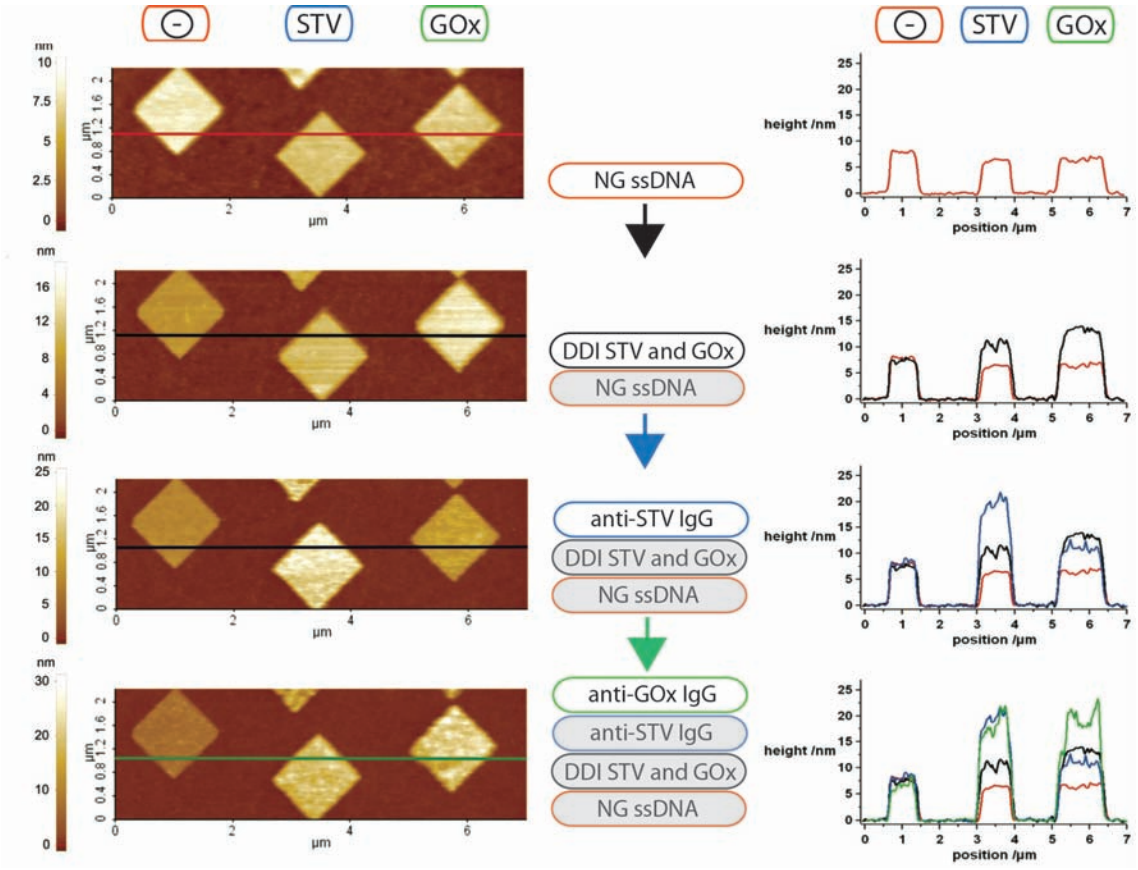

Figure 3.10: **Multiprotein nanoarrays *via* nanografting and DDI** - Use of nanografted oligonucleotide patches for specific immobilization of proteins and on their subsequent use for label-free detection of protein binding interactions.

on their respective complementary strands on the surface, as detected in the topographic profile. Two specific antibodies, anti-STV IgG and anti-GOx IgG dissolved in BISEKO (standardized human serum) matrix, were allowed to bind to this array, and each binding was monitored sequentially by topography measurements. The profile shown in figure 3.10 show clearly that both antibodies could be detected and no indication of nonspecific binding of either matrix components or target proteins disturbed these analyses.The observed specificity of biomolecular recognition and the lack of nonspecific binding confirm the suitability of nanografted patch arrays for applications in biosensing.

3.3.4 Nanografting of NTA-thiols: a platform of general applicability for his-tagged protein immobilization

NitriloTriacetic Acid terminated thiols borrowed the metal chelation affinity trapping of protein from purification protocol. Mixed SAM containing NTA-terminated thiols diluted in a EG matrix have been largely and successfully used for protein immobilization and binding studies (protein-protein interactions, protein-ligand interactions, (44, 46, 81)) through surface techniques, namely Surface Plasmon Resonance and its commercial devices like Biacore and IASys (49, 53). Preparation of these mixed monolayers was achieved from *in situ* chemical functionalization of SAM with NTA head groups or, more conveniently, from mixed solutions of NTA-terminated thiols in the form of $HS-(CH_2)_{16}-EG_3-NTA$ and a filler one, like, for example, EG_3-terminated thiols. Like all protocols for protein immobilizations, preparation of NTA SAM has to take into account many factor, like the miscibility of the thiols and the density ratio between the two molecules, so to maximize the number of binding site for the protein without posing steric hindrance concerns. NTA-surfaces are very attractive to surface biochemists'. Considerable amounts of extremely pure proteins are required for specific protein immobilization, request that is not easily fulfilled when protein are purified from biological specimen. The emergence of recombinant techniques for overexpression in suitable organisms equipped researchers with tools for quantitative production of desired proteins. As already mentioned in section 2.2.2.3 a mean for efficient purification and recovery of recombinant protein is the His-tag, a peptide easily fused to proteins virtually without

pitfalls. The imidazolic nitrogens of two histidines in the tag complete the octahedral coordination of Ni (II) trapped onto NTA, that with his three carboxylic acid and one nitrogen occupies the other four positions. This chelation is reversible and effectively displaced by histidines competitors, like concentrated imidazole solutions, so re-usability of the surface is possible. The affinity of this chelation was measured to be 10μM in solution, but the binding strength on surfaces increases at least tenfold, with a dissociation constant of 1μM. However, density of the NTA moieties on the surface is known to play a major role in the stability of the functionalized surfaces.

Affinity of NTA-thiols has been improved in recent years by Piehler and Tampe's group (54) with the use of multivalent chelator (MCHs) agents like thiols with multiple NTA headgroups (where "multivalent" refers to the global NTA moiety). Single component and EG_3 mixed SAM of mono-, bis- and tris- NTA-terminated thiols were extensively characterized by means of contact angle goniometry, ellipsometry, and infrared spectroscopy, showing superior properties of MHCs compared to monovalent chelators, and providing informations for a deep understanding of the effects of the charged and hydrogen bond accepting/donating within NTA groups on the packing of NTA-terminated thiols on solid surfaces.

Single component SAMs of NTA-thiols, whether mono- or multi- valent, show increasing density of thiols on the surface with increasing molar fraction of the same molecule in loading solution up to 80 mol%, above that the bulky NTA groups interact laterally upon formation of the SAMs on the surface, and a densely packed assembly of alkyl chains in an extended all-trans conformation is no longer possible. A contribution of disturbing lateral interactions between the EG_3-linker in between the chains cannot be excluded (45, 54).

EG_3 mixed SAM of mono-, bis- and tris- NTA-terminated thiols showed a critical molar ratio (in % terms) in the loading solution above which the disorder of the SAM and phase separation phenomena start to appear. Molar ratios 0-30 mol % of the NTA thiols with respect to the filling EG_3 molecule resulted in mixed MCH SAMs containing a densely packed alkyl layer, an amorphous ethylene glycol layer, and an outermost layer of NTA groups exposed to the ambient (54).

Valiokas et al. provided also a functional characterization of ligand (His-tagged proteins) binding kinetics and reversibility, showing that higher densities of NTA

trigger surface steric hindrance in protein immobilization, a phenomenon that is emphasized with the use of multivalent chelators; the same MCH are, on the other hand, offering a more stable surface. It was previously reported that long His-tags likely cover multiple NTA moieties, even when monovalent chelators are used, and that in the presence of higher density of NTA neighbouring groups rebinding effects contrast the dissociation of his-tagged proteins from the surface. A modulation of NTA-thiol density provides, therefore, a mean for tunable immobilization properties.

In contrast to spontaneous self assembly from solution, that requires a strong dilution of NTA-thiols into matrix thiols to yield ordered NTA-containing SAMs, nanografting offers a unique route to nanopatterned NTA-patches with high local concentration without compromising molecular packing and order, as already demonstrated for alkanethiols. For this thesis, we chose to nanograft monovalent NTA-EG_3-$(CH_2)_{16}$-SH[1] in a EG_3-$(CH_2)_{11}$-SH matrix. Ethanol solutions of NTA-thiol in the concentration range $14 \div 450$ μM were effectively nanopatterned; above that range, clustered aggregation of physisorbed and chemisorbed molecules was observed, while below that range, thiol substitution was inefficient. The nanostructured patches served for subsequent functionalization with two different his-tagged Fragment of antibodies that were able to provide oriented immobilization of recombinant mouse prion protein. Next chapter will detail the bichemical characterization of these nanostructured interfaces.

[1] kindly provided by prof. Jacob Piehler

4

Oriented PrP immobilization

We show here that nanografting enables to immobilize recMoPrP(89-230) in an oriented manner and to study its interactions by means of carefully executed topographic measurements on a very flat surface [1]. As a substrate, a very flat gold film covered by a monolayer of alkane-thiol supported triethyleneglycol serves as a reference which we call "the carpet".

After functionalization of the substrate with one of two different Fabs (antigen binding fragment of antibodies) and topographic measurements in Contact Mode (CM) AFM in a liquid environment, we were able to detect not only the successful recognition of recMoPrP(89-230), but also the two different orientations of the PrP in the two different orientations. The differential height increase (between two subsequent steps) over the nanopatches is in good agreement with the molecular size of the immobilized protein. To this end, we compared our experimentally determined topographic heights with previously published NMR and or crystal structures.

4.1 Experimental design

Metal complexes like Ni^{2+}-NTA are commonly used in affinity purification and immobilization strategies (52, 53), since they allow for reversible affinity capturing of histidine tagged proteins in a known orientation. Previously, micro and nanopatterning of NTA-functionalized SAMs have been exploited for oriented immobilization of

[1] Sanavio B., Scaini D., Grunwald C., Legname G., Scoles G., Casalis L., submitted to ACS Nano.

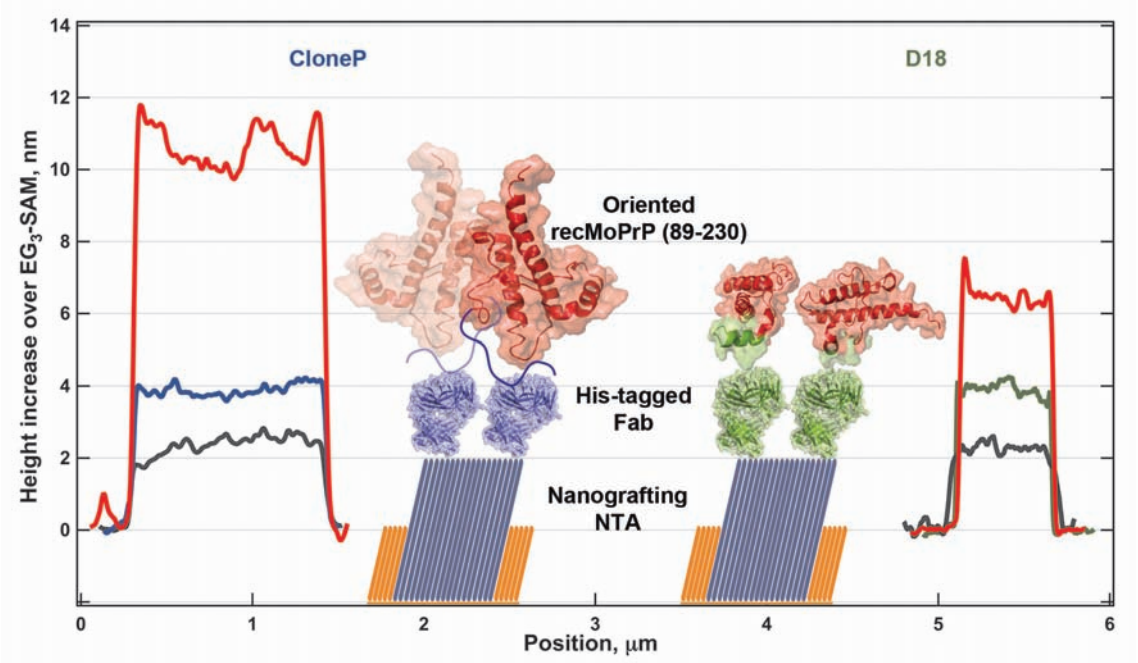

Figure 4.1: **Cartoon of the oriented immobilization of recMoPrP(89-230) on Fab-derivatized surfaces, with average height profile resulting at each step of the assay (pH 7.4).** - After nanografting of NTA-EG_3-C_{16}-SH into a reference carpet of protein repellent EG_3-C_{11}-SH, histidine-tagged Fabs (CloneP, on the left, and D18, on the right) are immobilized in different experimental runs taking advantage of His-tag-Ni-NTA interaction on the nanopatches. Afterward, the sample is incubated in a solution containing recMoPrP(89-230) 300nM. At each step of the assay, topographic measurements (CM-AFM profiles are reported here) are collected for each nanopatch. Protein models are based on previously published structures (e.g., see 1hh0.pdb, for Fab (82), and 1qm0.pdb, for recMoPrP (83)). RecMoPrP structures are drawn at the same scale when oriented on the two different Fabs; blue tail represents the unstructured part not resolved by NMR spectra, where CloneP binds, D18 epitope is colored in green.

targeted proteins (53, 54, 60). Here, however, by coordination of Ni^{2+}, two different histidine tagged recombinant Fabs, D18 and Clone P, were separately immobilized at controlled density and orientation, on nanopatches, allowing for optimized and oriented immobilization of the recMoPrP(89-230), a truncated recMoPrP that lacks largely of the unstructured N-terminal region. CloneP (70) and D18 (84) have been extensively studied in vivo and also in vitro in their binding properties towards PrP^C and PrP^{sc} and the recMoPrP. D18 recognizes the epitope spanning residues 132-156, that is considered important in the prion replication, while CloneP blocks a stretch of positively charged aminoacid spanning residues 95-105 in the very flexible N-terminal part.
Figure 4.1 reports an example of height profiles recorded with reference to the surrounding carpet of EG_3-thiols, and the specific height increase over the patch at each step is neatly recorded by AFM topographic measurements. Nanostructured surfaces were used to capture in controlled orientation recMoPrP(89-230) in two different buffer conditions to study the effect of pH on protein immobilization. At pH 7.4, at physiological condition, the two differently Fab functionalized surfaces were exploited as an immunoassay to capture the target recMoPrP(89-230) at different concentrations and to perform binding studies. At pH 5.8, near the pH at which the recMoPrP(89-230) is refolded after purification, we captured the protein on the functionalized nanostructures to detect by topography the effect of pH on the immobilization and on the recMoPrP itself, since effect of pH on conformation and charge distribution have been reported.

4.2 Topography Detection of Oriented Immobilization of recMoPrP(89-230)

After nanofabrication, NTA nanopatches (varying in size from $0.5 \times 0.5 \mu m^2$, 128 lines, and $1 \times 1 \mu m^2$, 256 lines) were functionalized with the two different Fabs at pH 7.4 in TBS (Tris Buffered Saline, 20 mM TRIS buffer, 150mM NaCl), that is compatible with the reported affinity studies(70, 84) on PrP both in vitro culture and with SPR (Surface Plasmon Resonance). Topographic measurements using CM-AFM were conducted to discriminate the orientation of the molecules.

4.2.1 Characterization of NTA-Nanopatches

NTA patches imaged in ethanol during the nanografting process showed a height increase over the carpet of 3.5 ± 0.4 nm (± Standard Deviation, S.D., as for other errors reported), in agreement with the theoretical difference expected from the molecule's theoretical length (85) (theoretical height difference is 3.5 nm, see Appendix 5 for further details).

In contrast to spontaneous self assembly from solution, that requires a strong dilution of NTA-thiols into matrix thiols to yield ordered NTA-containing SAMs (NTA thiol could be mixed only up to 30 mol%),34 nanografting offers a unique route to nanopatterned NTA-patches with high local concentration without compromising molecular packing and order, as demonstrated for alkanethiols (76).

The same patches imaged right after nanografting in TBS, however, showed a height increase of 2.3 nm ± 0.3 nm over the surrounding SAM (Figure 4.2). The carboxylic groups of the NTA moieties on the top of the supporting thiol (NTA-EG_3-C_{16}-SH) are ionized, and strongly negatively charged, at pH 7.4, so that electrostatic repulsion between adjacent head groups may induce relaxation or "opening" of the NTA head groups themselves, leading to an overall lower height. This observation was confirmed by studying the influence of the pH during imaging (see following sections) and by comparing the height of the patches right after fabrication in ethanol that is a less polar environment.

4.2.2 Characterization of Fab-finctionalized Nanopatches

Once derivatized with either D18 or CloneP, the surface of the patches did show a height increase of 2.0 nm ± 0.4 nm for D18 and 1.8 nm ± 0.3 nm for CloneP, suggesting both loose packing and tilted orientation of the antibody. In fact, looking at the molecular size taken from the structure of an analogue of CloneP (2hh0.pdb (82)), the Fab would present a long major axis of about 5.6 nm, assuming that it seats straight and extended over the patch. However, if the antibody fragment was free to rotate over the blocked histidine tail, just a slight inclination of the major axis would explain a measured height of half than expected, as the vertical projection of the

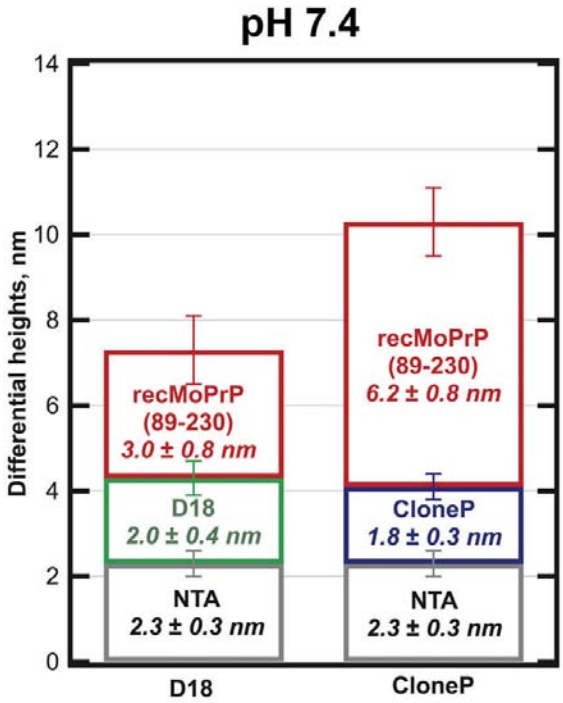

Figure 4.2: **Oriented immobilization of recMoPrP(89-230) at pH 7.4** - Oriented immobilization of recMoPrP(89-230) at pH 7.4 (20mM Tris, 150 mM NaCl) on D18 (left column) and CloneP (right column) functionalized patches. Differential height contribution relative to the NTA-thiol patch, the Fab immobilization (D18 or CloneP, respectively left and right), and recMoPrP are shown. All values are given $\pm$ Standard Deviation, (S.D.), as derived from two independent experiments of four nanopatches each.

molecule size is now smaller. Slight differences between the measured average heights of two Fabs, CloneP and D18, may be due to both differences in the two individual structures and in the packing during self-assembly over the NTA nanopatch.

Orientation specific docking of CloneP and D18 on NTA-nanostructures was immediately evident from topographic imaging of the surface (see Figure 3). Generally, we found that surface roughness provides an additional read out that can help identifying different protein-surface interaction scenarios. In case of specific interactions (see Figure 3), we found a clean EG_3-SAM with modest variation in roughness (R_q between 0.3 nm before any fabrication step, to the 0.6 nm average roughness of the surface at the end of the assay after recMoPrP immobilization). For a contaminated carpet due to unspecific protein interactions, we observed (in a few well identifiable occasions) a significant increase in roughness (>1nm). The roughness of the nanografted patch, that was relatively smooth at the NTA-fabrication step (on average, 0.6 ± 0.1 nm), increased as the Fab was immobilized, to 1.0 nm ± 0.3 nm for CloneP, while it remains constant around 0.6 nm ± 0.3 nm for D18.

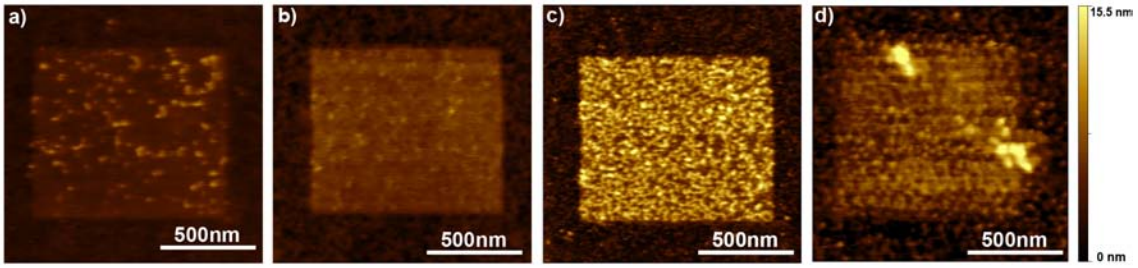

Figure 4.3: **Topography images in TBS pH 7.4 in CM-AFM.** - a) NTA nanopatterned at $1 \times 1\mu m^2$, 256 lines; b) same patch after CloneP immobilization; c) after recMoPrP immobilization (300 nM), and d) after regeneration with TBS 400mM Imidazole. Color scale is adjusted to be the same in all images.

4.2.3 Capturing recMoPrP(89-230) in selected orientation

The surfaces were challenged with a 300 nM solution of recMoPrP(89-230), a concentration high enough to ensure patch saturation. This concentration is in fact more than 100 times the known dissociation constants for both the two Fabs, thus

allowing for more than 99% fractional occupancy of the binding sites. As indicated by the increase in height, the two Fabs were able to recognize their antigen. From properly oriented molecules in structure (pdb) files, obtained from previously published mouse PrP NMR data (83, 86, 87), we expected an overall protein size of about 3 nm on the D18 functionalized patches, and of about 6 nm on the CloneP derivatized ones. These expectations were in very good agreement with the data shown in Figure 2. CloneP and D18 capture the recMoPrP(89-230) exposing different surfaces and different morphologies to the AFM tip: the two distinct increases in height are due to the oriented recognition of the PrP by the Fab-functionalized nanopatches and reflect the expected molecular size of recMoPrP, as 6.2 nm ± 0.8 nm over the CloneP-nanopatch and 3.0 nm ± 0.8 nm over the D18 functionalized structures.

To further confirm the extrapolated size with experimental data, another immobilization chemistry has been tested. RecMoPrP(89-230) was covalently linked to nanografted patches of carboxylic acid terminated thiols (HS-$C_1$5-COOH), activated to react with free amine groups of lysine side chains on the protein surface, giving an height of about 4 nm, but with a rough and inhomogeneous surface (see figure 4.4). The roughness was further enhanced by binding of D18 because, in this case,

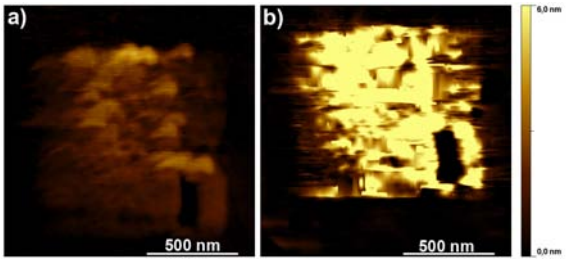

Figure 4.4: **Covalent immobilization of recMoPrP(89-230)** - a) Nanografted patches of (HS-$C_1$5-COOH), and b) covalent crosslinking of recMoPrP(89-230)

the proteins do not present all the binding sites oriented in the same way, so not all of them are available for recognition by the corresponding antibody.

4.3 Antibody/recMoPrP(89-230) Recognition as a Function of Protein Concentration: Apparent Binding Constant Measurements

4.3.1 Primary results

Biorecognition efficiency of recMoPrP on the two functionalized nanostructured interfaces was investigated through the estimation of apparent affinity constant (as apparent dissociation constant, K_{dapp}), after titration as a function of recMoPrP concentration. SPR affinity data were already reported in the literature(70, 84) for measurements at pH 7.4, the same condition we chose, and these data can be used to compare how nanofabrication and surface assembly may affect the immunoassay performance.

CloneP-functionalized surfaces were titrated against recMoPrP(89-230) concentrations ranging from 3 pM to 300 nM, and the average differential height increase due to deposition of the PrP molecules on the Fab functionalized patches was monitored. Differential height increase is related to specific binding onto the nanostructure and, of course, it increases as a function of the specific coverage on the spot. The height response (Δh) of recMoPrP, as well as the roughness signal, was used to estimate an apparent affinity parameter (see Figure 4).

The derived apparent affinity (K_{dapp}) of the molecule for the functionalized surface, that we measure to be 3 nM $\pm$ 1 nM (1.5 nM $\pm$ 1.3 nM from the roughness signal), equals or is up to 10 times larger than the estimated CloneP affinities for cognate epitope measured on macroscopic surfaces which ranges between 0.3 (hybrid mouse and bovine engineered protein), 0.5nM (Bovine peptide spanning residues 95-145), and 2.6 nM (Human peptide 95-145), as previous SPR characterizations reported (70). At a concentration of target equal to the K_d concentration, let's say 0.5 nM recMoPrP concentration in this case, on average half of the Fab molecule would be complexed, that is, half saturation is reached, and the response signal is proportionally decreased compared to the (almost) fully saturated one. We expect that, in addition to experimental error, the probably closer packing of the molecules induces the steric hindrance that is responsible for the deviation from the bulk surface value

(88, 89). Indeed the roughness signal, in our case connected to the coverage on the nanopatch surface, correlates slightly better with the results obtained on extended surfaces employing SAMs. We may argue, though, that SPR data, fast and useful on large scale studies, have actually little control over molecule orientation and many reports (6, 32, 88, 89) highlighted how this effect is actually underestimated in surface studies. Moreover, the data we are referring to, while providing very useful comparison for our novel assay, were obtained from surfaces functionalized in the opposite way: recMoPrP or shorter peptides were chemically linked on the surface, without any preferential orientation of the binding sites towards the Fab, that was added to the solution.

The same experiment was conducted on **D18-functionalized patches**, but in this configuration the shorter molecular size is offered as a signature of the recognition, and at low patch saturation the average differential height increase signal is too low to be detected with sufficient accuracy, in contact mode. At 3 nM recMoPrP, the increase in height registered by us on the patch is only of 1.5 nm $\pm$ 0.8 nm. Based on the affinity reported in the literature (84) (K_d 1.6 nM), we speculate that already in the low subnanomolar range the coverage is too loose to produce a reasonable signal. In fact, the Δh measured at 3 nM (2 times K_d) is half of the signal at 300 nM concentration, which is not very far from saturation. This implies that, in this configuration, at very low concentration, the PrP coverage could not be enough to generate a sufficiently high topographic signal.

4.3.2 Effect of Changing the Surface Coverage of the NTA Groups

Since the density of D18 and CloneP probes was expected to play a role in the biorecognition of recMoPrP, the NTA-patch nanofabrication was varied in the 14 to 450 μM range of grafting concentration, and scan density equal to 1.28 (half than the density used in the experiment above). After fabrication topographic height and roughness measurements were performed in both contact and non-contact mode (NC). We expected NC-AFM measurements to be much less perturbative on immobilized protein, since at low coverage proteins may be more prone to tip-induced

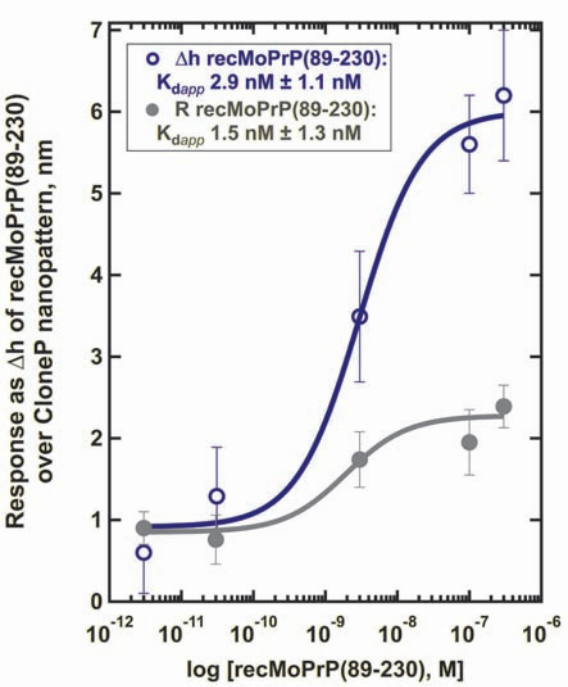

Figure 4.5: **Dose-response curve.** - Differential height (Δh recMoPrP, blue curve and open blue circle) contribution due to recMoPrP(89-230) binding on CloneP patches. A similar sigmoidal response is recognized from the roughness of the patch as a function of recMoPrP concentration (gray line, solid circle).

deformation. A test on a different buffer solution suitable for multiple pH measurements and compatible with protein immobilization was performed. Among the buffer solutions capable of covering a wider range of pH, a phosphate buffer 50 mM 150 mM NaCl was chosen.

Moving from neutral (7.4) to basic (8.0) pH for imaging purposes, the height of the NTA-nanopatch at equal fabrication parameters (density of lines and grafting concentration) decreased, confirming the trend of electrostatic repulsion between head groups of the molecules. When functionalizing the NTA nanopatch with CloneP in phosphate buffer pH 7.4, non contact (NC) measurements in liquid revealed a negligible increase in height, pointing to an extremely low density of probe. However, when titrating the surface with increasing concentration of recMoPrP (89-230), specific immobilization was achieved only on the patches, and the differential increase in height over the patch due to recMoPrP immobilization was following a sigmoidal trend, with an apparent affinity constant of 2.0 $\pm$ 0.8 nM and 1.6 $\pm$ 0.8 nM on patch fabricated at 450 μM and 143 μM NTA-thiol concentration, respectively (see Figure 5, panel a). At higher titer of CloneP (625 nM against the usual 300 nM) an increase of 1.2 nm was detected (on 450 μM NTA-patches), but negligible recogniton of recMoPrP(89-230) was achieved between 300 pM and 35 nM.

D18 was tested in the same condition (Figure 5, panel b). Despite a negligible signal of D18 functionalization, patches were responding specifically to increasing concentration of recMoPrP(89-230). Confirming contact mode measurements, saturation of the nanopatches was not achieved below nanomolar concentration, and apparent K_d estimation at 450 μM and 90 μM NTA patch fabrication were pointing to 2.9 $\pm$ 1.1 nM and 1.9 $\pm$ 1.3 nM, respectively, near the SPR data (84) (1.6 nM).

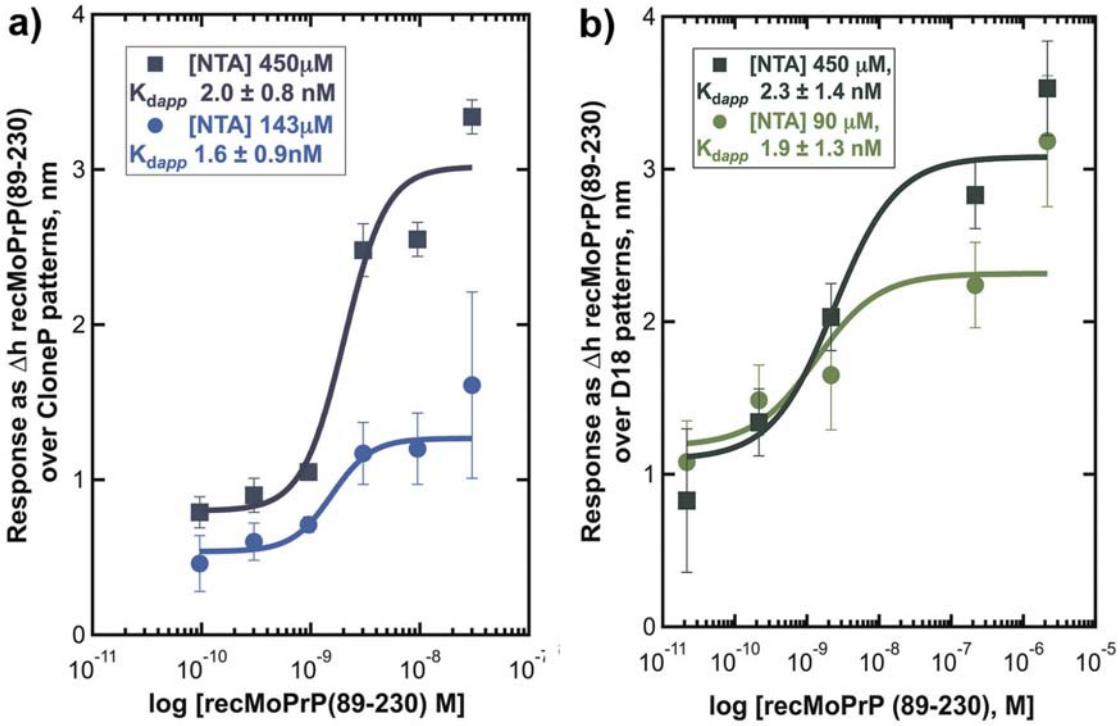

Figure 4.6: **Dose-response curve of differential height measured in NC mode** - Δh recMoPrP (blue curve and open blue circle) contribution due to recMoPrP (89-230) binding on CloneP patches (panel a) and D18 patches (panel b) as a function of NTA-thiol grafting concentration (scan density equal to 1.28, imaging buffer 50mM phosphate buffer, 150 mM NaCl, pH 7.4). The estimated $K_{d\mathrm{app}}$ decreases as the grafting concentration –and in turn, Fab density– decreases. However, especially for D18 functionalized patches, good S/N (Signal-to-Noise) ratios are achieved for NTA thiol concentration above 90 μM.

4.4 Effect of pH on recMoPrP Immobilization

In addition to the above experiments recMoPrP(89-230) was captured on Fab derivatized surfaces at pH 5.8 (20 mM sodium acetate buffer, 150 mM NaCl). This buffer is similar to the one used for refolding recMoPrP(89-230) into a stable Îś-helical rich conformation after purification (see Figure 2, panel b). Under these conditions, NTA patches showed a height increase of 3.2 nm ± 0.4 nm over the carpet, in agreement with the theoretical value of 3.5 nm, and suggesting a compact and ordered packing of the thiols, and a screening of the electrostatic repulsion of the head groups.

Initially, the surface was derivatized with either D18 or CloneP Fab at 300 nM concentration, showing a differential increase in height of 4.7 nm ± 0.4 nm for D18 and 3.5 nm ± 0.3 nm for CloneP, in improved agreement with the molecular size taken from previously published structures, indicating a more compact layer of probes than in the case of 7.4 pH, as shown in picture 4.7. The difference between the measured average heights of two antibodies increased, from 0.5 nm at pH 7.4 to 1.2 nm, suggesting a different response of the two molecules to pH variations. Specific and stable docking on the nanostructures was achieved also at pH 5.8, while the EG3-SAM remained clean during the assay as the modest variation in roughness confirmed (between 0.24 nm before any fabrication step, to the 0.6 nm average roughness of the surface at the end of the assay after recMoPrP immobilization). At the **NTA-fabrication step** the roughness of the patch remained relatively smooth (on average, 0.5 ± 0.1 nm in buffer). It increased as the Fab was immobilized, as 1.2 nm ± 0.4 nm for D18 and 0.6 nm ± 0.3 nm for **CloneP**, pointing at a possible lower coverage of the surface in the latter case and confirming the topographic height data. Subsequently, the patches were exposed independently to a 300 nM solution of recMoPrP(89-230), and the two Fabs were both able to recognize their antigen. We measured an average thickness of the recMoPrP layer of 3.6 nm ± 0.5 nm on the **D18** patches and of 4.9 nm ± 0.4 nm with the CloneP sublayer, (with a corresponding roughness of 1.8 nm and 1.1 nm, respectively). Despite the total height after target capture is almost the same on both patches (due to the different Fab contributions),

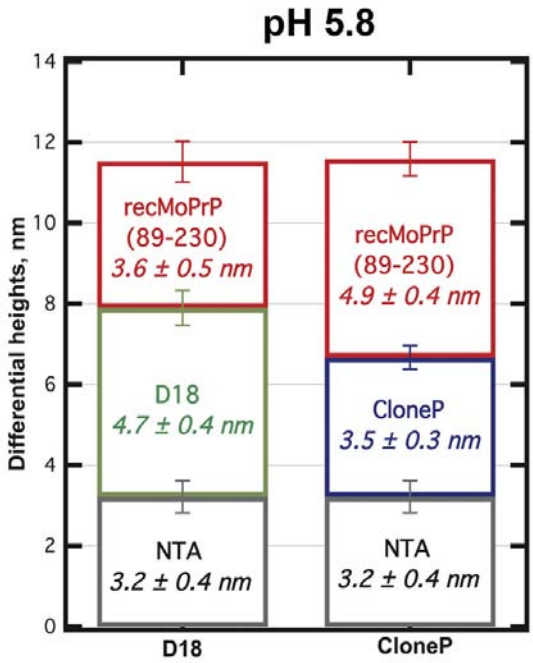

Figure 4.7: **Oriented immobilization of recMoPrP(89-230) at pH 5.8** - Oriented immobilization of recMoPrP(89-230) at pH 5.8 (20mM sodium acetate, 150 mM NaCl) on D18 (left) and CloneP (right) functionalized patches. Note how the decrease in pH affects the assembly of the molecule on the nanostructures. All values are given $\pm$ Standard Deviation, (S.D.), as derived from two independent experiments of four nanopatches each.

the actual increase due to **recMoPrP(89-230)** was still confirming the successful orientation of the protein and its detection through topographic measurements.

We tested same density NTA-nanopatches functionalized with a CloneP incubation concentration of 625 nM and the height increase due to Fab immobilization was 4.7 nm ± 0.2 nm. This value has to be compared with the 3.5 nm ± 0.3 nm obtained at 300nM CloneP concentration, which is consistent with a higher number of Fab molecules being immobilized at higher incubation concentration. However, the recognition of recMoPrP by the CloneP surface was definitely worse, since the recMoPrP layer thickness was only 1.6 nm ± 0.3 nm, suggesting the presence of steric hindrance. Moreover, considering the isoelectric point of PrP, near 9, and the uneven distribution of charges revealed at pH 4.5 by NMR (86), an electrostatic impairment to the proper assembly of PrP molecules on the Fab surfaces is expected to play role (86). A dramatic decrease in affinity of the antibody towards the recMoPrP can be safely excluded, since antibodies were extensively tested in cell culture and under physiological condition, and so was also excluded the instability of the chelating chemistry at this pH. In fact, pH 5.8 is more than one unit above the pKa of carboxylic acid, that contributes in their ionized form to the coordination of Ni^{2+}; on the other hand, the pK_a of bare histidines is 6.01 (85) that is, on average in this environmental condition, slightly more than half of the histidines presents one of the imidazole' nitrogen in protonated form and unable to coordinate the nickel ion. It is however known that the pKa of the imidazolic ring of histidines changes depending on the local environment condition, and that a high local density of NTA-Ni^{2+} moieties (like our case) favors a faster re-binding in case of transient dissociation of histidines (49).

Our nanostructured interfaces offer an extremely dense patch of NTA-thiols to the his-tagged proteins compared to conventional self-assembled NTA-monolayers (54), so that locally each his-tag is surrounded by a large molar excess of freely available NTA-moieties. A combination of these effects explains the observed stability of the Fab derivatized surfaces during measurements. In addition we want to point out that the binding of Fab did not occurred if the NTA patches were not loaded with Ni^{2+} ions, and that bound his-tagged probes were specifically displaced by imidazole washing (acetate buffer supplied with 400 mM imidazole).

4.5 Towards a versatile parallel platform

The experiments described so far were performed immobilizing either CloneP or D18 in an independent manner, because NTA-Ni-His-tag system is not suitable to simultaneous immobilization of His-tagged proteins at the very same time in multiple location: all the His-tags would recognize indifferently all the NTA-patterns, unless a precision deposition devices are used. Once functionalized with a single antibody, however, specific patterns can be regenerated locally, allowing for the creation of a device in which the two His-tagged Fabs are immobilized side by side in a parallel format.

Total regeneration of the surface can be achieved after extensive washing with a 400mM imidazole solution, followed by EDTA cleaning, that ensures the removal of His-tagged bound proteins by competition, or by scanning repetitively the whole pattern (or a selected area) at a loading force between 3 to 5 nN, and subsequent rinsing in buffer. As already mentioned by Tinazli et al. (60), erasing molecule from a NTA-functionalized monolayer doesn't alter its capture properties, and the area can be re-functionalized with another His-tagged protein.

We exploited this technique to immobilize in a parallel manner the two antibodies on the very same surface, side by side, in order to confirm the two binding configuration of recMoPrP (89-230), to study the phenomenon as a function of density on the very same surface. We chose pH 5.8 to achieve a more efficient regeneration of the patches. In addition, we tested the prion protein functionalized surface as a platform for additional biochemical studies such as the study of enzymatic digestion of proteins.

An array of NTA-nanopatterns was nanografted varying the density of grafting lines within each pattern. An example of such array is given in figure 4.8. In this way the local density of NTA within each line is the same, since it depends only on the grafting concentration when the grafted lines do not overlap, but the efficiency of substitution in the overall area of the pattern is changed as the tip "writes" fewer lines. Pairs of patches were produced with the same density, with ratio between

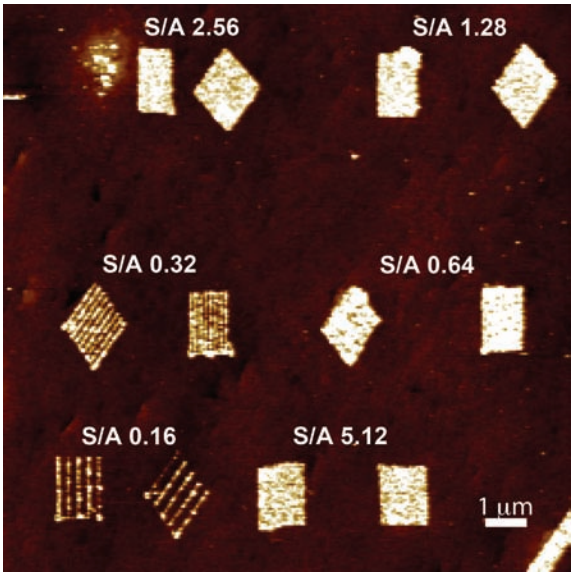

Figure 4.8: **Multidensity array.** - Pairs of patches have been nanografted at variable surface density ratio.

scanned and actual area of the pattern ranging from below one (separated lines i.e. the regime described above) up to where each portion of the surface was "written over" 5.12 times, were produced.

Patterns were functionalized with D18 Fab, measured, then at each density D18 Fab was "tip-erased" from one of the two patterns (as shown in figure 4.9, and the regenerated surface was measured and re-functionalized with CloneP. The array presented pairs of equal density patterns, one derivatized with D18 and one derivatized with CloneP. Binding of recMoPrP (89-230) 300nM was followed on both antibodies and at different densities. The Δh due to rec MoPrP (89-230) in the two configurations is presented in figure 4.10 a and b: while the Δh over CloneP smoothly increase increasing the density, recMoPrP (89-230) suffered at higher density of probes when oriented on D18. The accessibility of binding sites affects the biorecognition and therefore is dependent on packing. CloneP recognizes an epitope on the portion of the unstructured N-terminal part of the prion protein: by immobilizing via CloneP the truncated PrP, the small portion of this flexible arm was hidden to the solution and the surrounding molecules. This portion is not masked on D18-functionalized

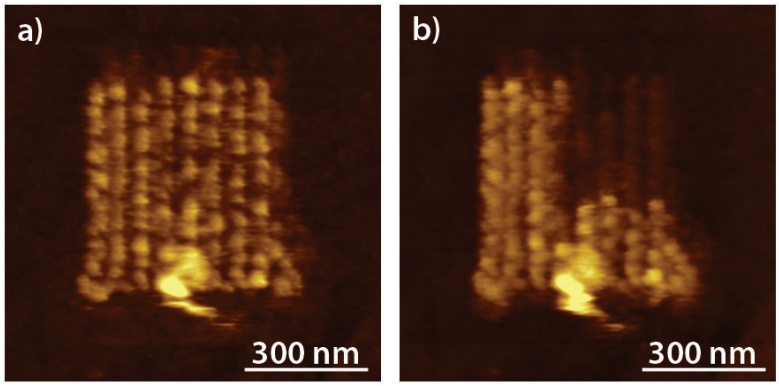

Figure 4.9: **Tip-mediated patch regeneration.** - Scanning at moderate force and higher speed, patches can be cleaned and the NTA functionality is presented afresh for another immobilization step.

patterns and possibly its fluctuations in time and space ask for a different reorganization of the proteins molecules on the nanopattern, were the local concentration of molecules was very high. Moreover, the charge distribution at low pH (4.5) revealed by NMR (86) on human prion protein was uneven –it almost showed two differently charged "faces"– and suggested an electrostatic repulsion contribution to the assembly on the nanopattern).

Enzymatic reaction The nanoarrays were then regenerated via Proteinase K (PK) treatment. PK is a serine protease, an enzyme that catalyzes digestion of a broad spectrum of proteins, used to discriminate the misfolded core of PrP^{sc} since it is resistant to PK treatment. PK treatment of the nanopattern was supposed to regenerate the whole array (both refolded recMoPrP and Fabs are substrates for the PK enzyme), at slightly different rate depending on the total amount of protein on each nanopattern, as shown in figX: after 1.5 hrs, low density patch were already regenerated to the (almost) clean NTA-surface, while higher density pattern were still unhomogeneously rough (roughness rising from 1.6 nm at lowest density and 3.8 nm at higher density) and their height revealed a thick layer of protein deposited. After additional 14 hrs, almost all the patches were regenerated to the NTA level. Eventually, a time controlled PK digestion on surface in which a mixture of PrP^{c} and PrP^{sc} is captured, like from biological specimen, would serve as a tool to identify on

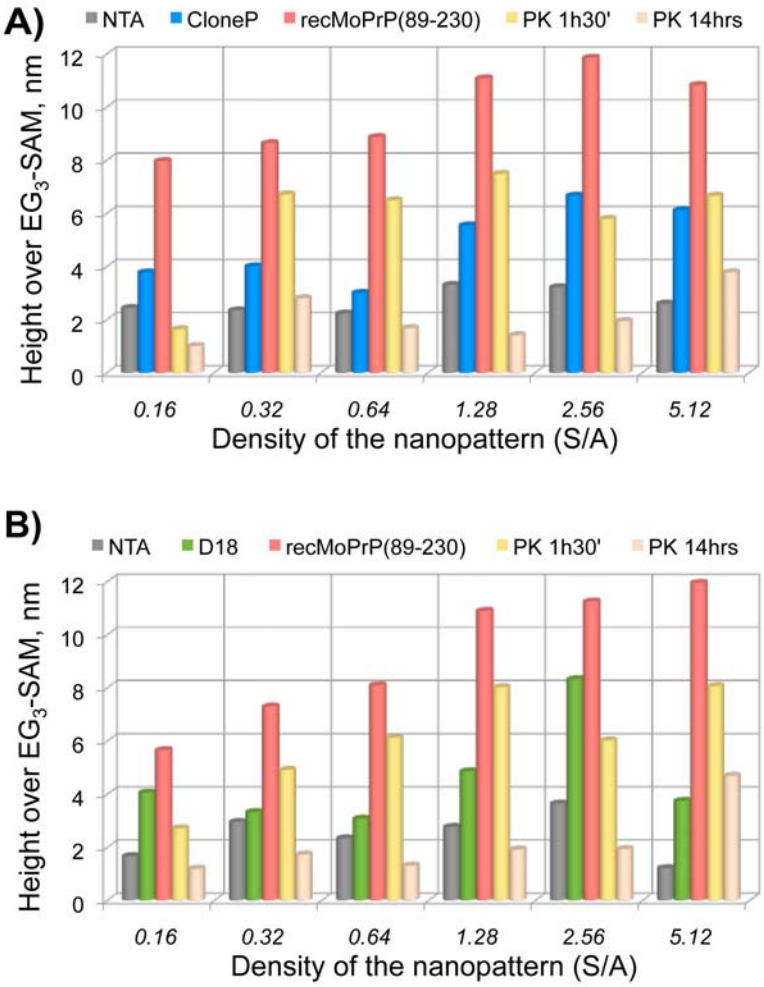

Figure 4.10: **Pseudoparallel assay configuration.** - A pseudo parallel assay is performed: after D18 functionalization, one of the pattern per each pair was "cleaned" by scanning at moderate force and higher speed CloneP was immobilized on the free nanopattern. Panel a) and b) show respectively the results on D18-functionalized patterns and CloneP functionalized patterns, and the proteinase two step cleaning as a function of nanopattern density: the decreasing number of fabrication lines reduces the total amount of protein immobilized and the proteolytic cleavage is more efficient.

the nanopatches the region in which the misfolded prion resistant to PK digestion is immobilized.

5

Perspectives

We have demonstrated the oriented immobilization of recMoPrP molecule at the nanoscale and the measurement of the effect of confinement on biorecognition combining nanografting, bioaffinity immobilization and differential height measurements using an AFM based platform. Nanografting has been used previously (61, 62, 63, 65, 66, 67, 76) to study the effect of patterning of protein on the surface in different configurations, but with very little attention on the performance of the bound macromolecules in a recognition-based assay. The specific receptor protein orientation has to be homogeneous, the surface roughness should not mask or affect the binding site accessibility from the solution and the incubation times have to be sufficiently long to approach equilibrium and to be chosen accordingly to the characteristic kinetic constants of the molecule under investigation. In this way the performance of the nanostructured surface can be tested in a quasi-quantitative assay.

Nanografting of NTA-terminated thiol provides a very general route for specific protein immobilization in a controlled orientation, since the polyhistidine tag can be genetically engineered in recombinant protein in a known position, and the interaction with Ni-NTA complex is specific. Moreover, this immobilization is reversible and ensure re-usability of the surface. The nanografted NTA-Ni-His-tag system on a flat protein repellent reference carpet generates an homogenous surface in which the His-tagged fragments of antibodies are immobilized to maximize the distribution of the binding sites towards the solution containing the target protein. Choosing

Fabs, like D18 and CloneP, allowed for the orientation of recMoPrP(89-230), since their binding sites are on different locations on the PrP surface. The two different configurations (CloneP immobilized recMoPrP(89-230) and D18-immobilized recMoPrP(89-230)) are discriminated by accurate measurements of the molecular size of the protein.

The minimum signal detectable from recMoPrP(89-230) binding was in the tens of picomolar, a value that depends less on diffusion-limited kinetics than on the affinity constant of the antibody, the latter, being in the subnanomolar range, does not allow for saturation of the nanostructure in the low picomolar range. Unfortunately, due to safety concern, we couldn't test our devices with infectious prion sample. Nonetheless, we expect that a highly controllable surface with specific protein orientation would be very useful in the reliable testing of recognition and binding between biomolecules. Even though infectious prion concentration in peripheral blood and tissue is reported to be in the low fM range, successful detection with subnanomolar affinity antibodies could still be possible after proper sample treatment, like Protein Misfolding Ciclic Amplification (PMCA) (90), or specific sample increased concentration that, combined with the low volume consumption of this assay, would circumvent diffusion and affinity limits of the system. Finally we would like to note that our AFM-based tools have still an enormous potential, as we can speculate that converging efforts on parallel functionalization, diffusion enhancing system, centrifugal molecule focussing, high affinity antibody and last but not least tethered double binding molecules could further lower detection limits. A practical and lower cost version of our device will rest instead on the application of an easier to multiplex electrical readout system.

In addition to possible diagnostics applications, the strict control over PrP orientation opens many avenues of investigation of possible interacting partners, from large macromolecular complexes to small organic dyes that interact unconventionally with unfolded proteins (91) and may serve as a platform for protein misfolding studies on PrP and other thermodynamically unstable proteins. In particular, this oriented nanoconfinement of PrP, whether in its truncated or full lenght from, can be used for *in situ* fibrillation studies, in which the early stage of aggregation can

be followed in real time with high sensitivity as a function of multiple variable in a highly controllable environment. The use of antibodies that mask different regions of the PrP offers the advantage of understanding the assembly and interaction of proteins during fibrillation by varying the exposed region of the protein available for protein interaction. Other unstructured proteins, like α-synuclein, β-amyloid peptide, hungtintin,(92), offer intriguing example to test how the nanoconfinement can provide a useful, highly controllable environment for misfolding and aggregation studies on surfaces.

The expertise acquired during the completion of this thesis is now the point of departure for an integrated approach to nano-confinement of unstructured proteins as the substrate for a novel approach to biochemical characterization.

Technically, the know-how for both DNA and NTA nanografting based protein immobilization will be combined to exploit the extreme selectivity and parallelizability of the former with the versatility of the latter. Specifically, we are now using a ssDNA-NTA conjugate, kindly provided by Dr. L. Fruk (Karlsrhue University, Germany), to transform our nanografted DNA arrays into a protein platform with the added opportunity to immobilize in an oriented manner through the histidine tag an enormous variety of proteins. The delicate step in this new protocol is the careful preparation of the Protein-His-Tag Ni^{2+}-NTA-ssDNA complex in such a way that both the Ni^{2+} and the ssDNA do not promote and participate in any unspecific interaction with the target protein. Our preliminary results are suggesting that few percentage of imidazole and salt concentration (NaCl) above 150 mM help in preventing unspecific interactions when complexes with CloneP or N-terminal His-tagged-α-synuclein are involved and condition are being optimized and compared with the standard NTA protocol. Multiple mutant of α-synuclein can then be immobilized on the same surface (thanks to the specificity and selectivity of DNA hybridization) and then tested, for example, for the binding with new drug lead.

As the work of Staii (61, 65) successfully demonstrated, AFM can detect the binding of small molecule monitoring the variation in the frictional force between the tip and the protein as the ligand binds, over a large dynamic range of concentration. It could be very helpful in characterizing interaction involving "non conventional"

binding sites (that is, the lack of a well defined binding cleft, suggesting either a conformational rearrangement to create the pocket or a "diffuse" location distinguished only by the nature of the intermolecular force involved, or both). The presence of an unstructured protein, like α-synuclein, that can experience extreme fluctuation in conformation, introduces higher degree of complexity in the application of lateral force microscopy to the screening of potential ligands. Nevertheless, we expect that the use of friction force microscopy will reveal with enhanced sensitivity the binding of molecules like dopamine to α-synuclein, and by reflecting the proximity interaction between tip and sample, transient intra- and inter-molecular interaction will be detected.

We are also aware that the presence of a divalent transition metal ion may be the source of uncontrolled influences on the folding and on the surface deposition itself when IDPs are involved (as metal cation are known to interfere with them), so we aim at linking α-synuclein to gold *via* the introduction of a cysteine tag, too. Last but not least, in the framework of characterizing protein-ligand interactions through interfacial properties, we plan the use of SAM to supply an artificial lipid membrane for the study of α-synuclein interaction with lipids and lipid induced refolding, and eventual oligomer-driven pore-membrane formation. α-synuclein, implicated in the etiology of Parkinson's disease, shows an intrinsically disordered free state, characterized in its conformational pathway *via* Force Spectroscopy studies (93, 94), and *via* surface characterization of oligomeric states, and with a profusion of *in vitro* and *in vivo* techniques. Upon self assembly into fibrils or binding to lipid membranes or detergent micelles partial order, residual secondary structure and transient long-range interactions within the free state can be detected and may influence alpha-synuclein aggregation pathways. We expect that confinement at the nanoscale in controlled microenvironment of this protein may bring forth new and, perhaps, unexpected details that can help elucidating puzzling and obscure aspect of its physiological and pathological role.

Methods

Materials and Instrumentation

EG_3-thiols (HS-$(CH_2)_{11}$-EG_3-OH, 2-2-[2-(1-mercaptoundec-11-yloxy)-ethoxy]-ethoxy-ethanol) was purchased from Prochimia Surfaces (Poland), NTA-EG_3-$(CH_2)_{16}$-SH (2-2-[2-(1-mercaptohexadec-16-yloxy)-ethoxy]-ethoxy-ethoxy nitrilotriacetic acid) was kindly provided by Jacob Piehler. NaCl, imidazole, EDTA, $NiCl_2$, TRIS, sodium phosphate dibasic, potassium phosphate monobasic, ethanol (99.8% purity) were all provided by Fluka and Sigma Aldrich, (Milan, Italy). All the solutions were prepared in ultrapure 18.2 MΩcm water (Milli-Q, Millipore SpA, Milan, Italy), and filtered with a sterile syringe-filter (0.22 μm) immediately prior to use. All other reagents were of analytical grade. All AFM experiments were carried out with conventional AFMs using a XE-100 (Park System, former PSIA, Korea) working in contact mode; Non-Contact mode measurements in liquid were performed on a MFP3D Stand Alone AFM, (Asylum Reasearch, Santa Barbara, U.S.A.). For nanografting and NC-AFM imaging, commercially available silicon cantilevers (NSC19, Mikro-Masch, Poland, nominal spring constant $0.6\frac{nN}{nm}$, tip radius <10 nm) were chosen. For CM-AFM imaging purposes, a soft cantilever (CSC38B, MikroMasch, Poland, nominal spring constant $0.03\frac{nN}{nm}$, tip radius <10 nm) was used.

Protein Production and Purification

The Fabs, D18 and CloneP, were produced as previously reported with a (His-Gly)6 tag (70, 84). The recMoPrP(89-230) was produced and purified as reported previously(10). All the protein stocks were kept on ice if needed and diluted immediately prior to use.

Substrate and Monolayer preparation

Ultra flat gold films substrates were prepared using a modified Ulman procedure (40, 41, 43). Briefly, freshly cleaved mica sheets (clear ruby muscovite, Goodfellow Cambridge Limited, Huntingdon, England) were mounted in an electron beam gold evaporator and gold films were deposited at a rate of ∼0.1 nm/s and a chamber pressure of about 10^{-6} mbar until a thickness of 100 nm was reached. Small amount of SU8-100 (MicroChem Corp., MA, USA) polymer were then equally dropped on the gold side of the gold-mica sheet, and the polymer was then cured (baked 5 hours at 95° C, exposed 20 minutes under a 70 μW/cm2, 462 nm UV lamp, and baked at least hours at 95°C, sample for contact mode measurements).

With a similar approach, gold was evaporated on silicon wafers (University Wafers, MA, USA). Then, cleaned silicon slides of 5×5 mm^2 were glued to the gold surface using small amount of SU8-100, that was cured a few hours at 135°C. The SU8-drop, now looking as a flat hard surface strongly attached to the gold layer, can in this way be mechanically detached in air from the mica substrate, keeping the gold film attached to it and exposing now the gold surface originally buried at the interface with the mica. Such Au film surface has the advantage of reproducing the flatness of mica, giving an extremely reduced roughness of about 4Å(even when evaporated on silicon).

Samples are, immediately after stripping, soaked in a freshly prepared 300 μM solution of EG_3-thiol in ethanol. The substrates were kept in the thiol solution overnight in the dark at room temperature. In this way an ultra flat surface covered with EG_3-terminated thiols was obtained. AFM test measurements confirmed a roughness in the range of 3-4 Å.

The Nanofabrication Process

. In all the experiments the process of nanografting was performed in the following steps.

- (a) A freshly prepared SAM substrate was mounted in a closed liquid cell. Prior to grafting a worn out cantilever was used to scratch a sign into the gold

surface, that allows the optical alignment of the cantilever to a coordinate system which facilitates finding back the nanopatches.

- (b) The liquid cell was filled with the nanografting solution (e.g. a 450 μM NTA-thiol HS-$(CH_2)_{16}$-EG_3-NTA) solution. The SAM was imaged in liquid at low load to select the area where to fabricate the nanostructures.

- (c) The desired patches were obtained within the SAM by scanning the AFM tip above a threshold of about 70 nN, with a scan rate of 2 Hz. In this way the alkylthiol SAM phase was locally disrupted and immediately exchanged with the NTA-thiol monolayer phase. Varying the number of lines scanned by the tip during the nanografting patterning varies the actual area scanned by the tip (and where the substitution takes place): the area effectively substituted is estimated as the ratio between the area scanned (given by the contact area of the tip —10 nm— by the number of scanned lines) and the image area: $R_{tip} \cdot lines/area$. The best homogeneous NTA-patches were produced with a patch size of 500×500 nm^2 (i.e. 128 lines S/A 2.56) or 1×1 μm^2, (256 lines, S/A 2.56), and a scan rate of 2 Hz.

- d) After the grafting procedure, the patches were imaged in ethanol and afterward in buffer (with a soft cantilever and at low forces, namely below 0.3 nN) in order to record topographic, i.e. height, data. Size of the patches was chosen to be between 0.25 μm^2 and 1 μM^2.

Pattern Functionalization

After the nanofabrication process the surface was throughly rinsed with ethanol and dried. The sample was first washed with a 0.5 M EDTA (EthyleneDiamineTetraAcetic Acid, pH 8.6, Fluka) solution in order to remove undesired metal ions, with three washing step of 4 min each, and a solution containing 10 mM $NiCl_2$ (Fluka) in 20 mM TRIS, pH 7.4 (Fluka), was loaded on the sample for 5 min. The surface was then ready for the immobilization of the histidine tagged Fab âĂŞ–CloneP or D18–âĂŞ able to recognize the recMoPrP(89-230). The Fab has been added into the AFM liquid cell as a 300 nM solution in 20 mM TRIS 150 mM NaCl (Fluka) buffer

(pH 7.4) for 20 min. Height measurements revealed the presence of higher patches on the surrounding surface. No Fabs immobilization was achieved if the NTA surface was not loaded with Ni(II). Once the surface was functionalized and characterized, it was incubated at room temperature in a solution containing recMoPrP(89-230) at 300 nM concentration for 30 min. The presence of the molecule was then ascertained through height measurements after rinsing the surface in buffer.

Regeneration of the surface (removal of the PrP and the Fab) was achieved copiously washing with a solution of 0.4 M imidazole (Fluka) in 20 mM Tris buffer, and a subsequent washing step with EDTA 0.5 M was performed. The surface was then ready for another cycle of immobilization and assay measurements. Enzymatic surface regeneration was performed incubating the surface with a 100 μg/mL (50 mM Tris, 10 mM CaCl2, pH 7.4) Proteinase K solution (recombinant, PCR grade, La Roche Diagnostics, Germany) for 90 min and 14 hours. Regeneration of the surface through denaturation of the interaction between the Fabs and the recMoPrP, with either low pH (pH 4) or denaturant (4M urea) treatment, was abandoned since it was damaging the surrounding EG_3-carpet. In the case of covalent immobilization of recMoPrP, HS-C_{15}-COOH 100 μM was nanografted into EG_3-thiol. Then, the surface was activated for 15 min in a solution containing 5 mM DCC (N,N'-dicyclohexylcarbodiimide) and 15 mM NHS (N-Hydroxysuccinimide) in Tris Buffer 20 mM, pH 7.4, and then incubated for 50 min with a 216 nM solution of recMoPrP (89-230) or a 30 nM solution.

Binding Studies

Different concentrations of recMoPrP(89-230) above and below the K_d (0.5 nM) of each antibody were tested, and the differential height were used as the response signal and fitted to a three parameter sigmoidal dose response equation in Igor Pro (Wavemetrics, Inc.) through Visual Enzymics 2010 (Softzymics, Inc., NJ, USA). The topographic measurements were performed after an incubation in the recMoPrP(89-230) solution long enough to reach equilibrium. The incubation time was estimated as previously discussed in section 2.3.2.

Image Analysis

Each experiment involves the fabrication of multiple patches that contribute to the single experiment statistic, and to the inter-experiments statistics. All height measurements are reported with their standard deviations. Topographic images of the patches are then analyzed in term of pixel distribution (region analysis) in order to get the height value related to the patch at each single step of the experiment (nanografting, Fab functionalization, recMoPrP loading, regeneration step). The AFM instrument proprietary software (XEI, Park System, and MFP3D, Asylum Research) and free open source software, Gwyddion (`www.gwyddion.net`), were used. The experimental value was then compared to the global size of the molecule as obtained from pdb files (1hh0, for Fabs, 1ag2.pdb, 1qm0.pdb for recMoPrP(89-230), visualized with PyMol, Schrodinger, LLC., `http://www.pymol.org`).

The height of the patches is the relative height increase due to the nanostructure compared to the surrounding reference surface (SAM). Then, this height increase can be related to the fabrication and the recognition events that take place on the sensor surface as a differential height measurement. For example, the NTA patches are 2.3 $\pm$ 0.3 nm taller than the surrounding SAM (compatible with theoretical height: from CRC Handbook of Chemistry and Physics, (85)) bond length value were computed and corrected by the bond angle between Au-S-C and C-C-C of 109.5° and by the tilting of 30° of thiols in self assembled monolayer: a 3.5 nm difference). After the immobilization of the Fab, the patches are now 4.1 nm higher than the reference carpet. This relative height increase is due both to the contribution of the NTA-thiols (2.3 nm) and the Fab (4.1 nm $-$ 2.3 nm = 1.8 nm). Error was propagated as geometric sum.

References

[1] S B Prusiner. Prions. *Proc Natl Acad Sci USA*, 95(23):13363–83, Nov 1998.

[2] F E Cohen and S B Prusiner. Pathologic conformations of prion proteins. *Annu Rev Biochem*, 67:793–819, Jan 1998.

[3] P Brown, L Cervenáková, and H Diringer. Blood infectivity and the prospects for a diagnostic screening test in creutzfeldt-jakob disease. *J Lab Clin Med*, 137(1):5–13, Jan 2001.

[4] Rhiannon L C H Huzarewich, Christine G Siemens, and Stephanie A Booth. Application of "omics" to prion biomarker discovery. *J Biomed Biotechnol*, 2010:613504, Jan 2010.

[5] I Zerr, K Kallenberg, D M Summers, C Romero, A Taratuto, U Heinemann, M Breithaupt, D Varges, B Meissner, A Ladogana, M Schuur, S Haik, S J Collins, Gerard H Jansen, G B Stokin, J Pimentel, E Hewer, D Collie, P Smith, H Roberts, J P Brandel, C Van Duijn, M Pocchiari, C Begue, P Cras, R G Will, and P Sanchez-Juan. Updated clinical diagnostic criteria for sporadic creutzfeldt-jakob disease. *Brain*, 132(Pt 10):2659–68, Oct 2009.

[6] Christer Wingren and Carl A K Borrebaeck. Progress in miniaturization of protein arrays–a step closer to high-density nanoarrays. *Drug Discov Today*, 12(19-20):813–9, Oct 2007.

[7] Jamil Kanaani, Stanley B Prusiner, Julia Diacovo, Steinunn Baekkeskov, and Giuseppe Legname. Recombinant prion protein induces rapid polarization and development of synapses in embryonic rat hippocampal neurons in vitro. *J Neurochem*, 95(5):1373–86, Dec 2005.

[8] R Riek, S Hornemann, G Wider, R Glockshuber, and K Wüthrich. Nmr characterization of the full-length recombinant murine prion protein, mprp(23-231). *FEBS Lett*, 413(2):282–8, Aug 1997.

[9] Giuseppe Legname, Ilia V Baskakov, Hoang-Oanh B Nguyen, Detlev Riesner, Fred E Cohen, Stephen J DeArmond, and Stanley B Prusiner. Synthetic mammalian prions. *Science*, 305(5684):673–6, Jul 2004.

[10] Maurizio Polano, Alpan Bek, Federico Benetti, Marco Lazzarino, and Giuseppe Legname. Structural insights into alternate aggregated prion protein forms. *J Mol Biol*, 393(5):1033–42, Nov 2009.

[11] Jozef Adamcik, Jin-Mi Jung, Jérôme Flakowski, Paolo De Los Rios, Giovanni Dietler, and Raffaele Mezzenga. Understanding amyloid aggregation by statistical analysis of atomic force microscopy images. *Nature nanotechnology*, 5(6):423–8, Jun 2010.

[12] N Leigh Anderson, Malu Polanski, Rembert Pieper, Tina Gatlin, Radhakrishna S Tirumalai, Thomas P Conrads, Timothy D Veenstra, Joshua N Adkins, Joel G Pounds, Richard Fagan, and Anna Lobley. The human plasma proteome: a nonredundant list developed by combination of four separate sources. *Mol Cell Proteomics*, 3(4):311–26, Apr 2004.

[13] CM Perou, T Sørlie, MB Eisen, M van de Rijn, SS Jeffrey, CA Rees, JR Pollack, DT Ross, H Johnsen, and LA Akslen. Molecular portraits of human breast tumours. *Nature*, 406(6797):747–752, 2000.

[14] JD Wulfkuhle, LA Liotta, and EF Petricoin. Proteomic applications for the early detection of cancer. *Nature reviews cancer*, 3(4):267–275, 2003.

[15] Lee Hartwell, David Mankoff, Amanda Paulovich, Scott Ramsey, and Elizabeth Swisher. Cancer biomarkers: a systems approach. *Nat Biotechnol*, 24(8):905–8, Aug 2006.

[16] Dawn Mattoon, Gregory Michaud, Janie Merkel, and Barry Schweitzer. Biomarker discovery using protein microarray technology platforms: antibody-antigen complex profiling. *Expert review of proteomics*, 2(6):879–89, Dec 2005.

[17] SH Diks and MP Peppelenbosch. Single cell proteomics for personalised medicine. *Trends in Molecular Medicine*, 10(12):574–577, 2004.

[18] M Schena, D Shalon, R W Davis, and P O Brown. Quantitative monitoring of gene expression patterns with a complementary dna microarray. *Science*, 270(5235):467–70, Oct 1995.

[19] Yuichi Taniguchi, Paul J Choi, Gene-Wei Li, Huiyi Chen, Mohan Babu, Jeremy Hearn, Andrew Emili, and X Sunney Xie. Quantifying e. coli proteome and transcriptome with single-molecule sensitivity in single cells. *Science*, 329(5991):533–8, Jul 2010.

[20] JRS Newman, S Ghaemmaghami, J Ihmels, DK Breslow, M Noble, JL DeRisi, and JS Weissman. Single-cell proteomic analysis of s. cerevisiae reveals the architecture of biological noise. *Nature*, 441(7095):840–846, 2006.

[21] PT Spellman, G Sherlock, MQ Zhang, VR Iyer, K Anders, MB Eisen, PO Brown, D Botstein, and B Futcher. Comprehensive identification of cell cycle-regulated genes of the yeast saccharomyces cerevisiae by microarray hybridization. *Molecular biology of the cell*, 9(12):3273, 1998.

[22] Paul F Predki. Functional protein microarrays: ripe for discovery. *Curr Opin Chem Biol*, 8(1):8–13, Feb 2004.

[23] P Mitchell. A perspective on protein microarrays. *Nature biotechnology*, 20(3):225–229, 2002.

[24] Jan Kerschgens, Tanja Egener-Kuhn, and Nicolas Mermod. Protein-binding microarrays: probing disease markers at the interface of proteomics and genomics. *Trends in molecular medicine*, 15(8):352–8, Aug 2009.

[25] A I Archakov and Yu D Ivanov. Analytical nanobiotechnology for medicine diagnostics. *Mol Biosyst*, 3(5):336–42, May 2007.

[26] David H Geho, Alessandra Luchini, Enrico Garaci, Claudio Belluco, Emanuel Petricoin, and Lance A Liotta. Nanotechnology in clinical proteomics. *Nanomedicine (Lond)*, 2(1):1–5, Feb 2007.

[27] M Lynch, C Mosher, J Huff, S Nettikadan, J Johnson, and E Henderson. Functional protein nanoarrays for biomarker profiling. *Proteomics*, 4(6):1695–1702, Jan 2004.

[28] Stephen F Kingsmore. Multiplexed protein measurement: technologies and applications of protein and antibody arrays. *Nature reviews Drug discovery*, 5(4):310–20, Apr 2006.

[29] Carl A K Borrebaeck and Christer Wingren. Design of high-density antibody microarrays for disease proteomics: key technological issues. *Journal of proteomics*, 72(6):928–35, Aug 2009.

[30] RP Ekins. Ligand assays: from electrophoresis to miniaturized microarrays. *Clinical chemistry*, 44(9):2015, 1998.

[31] Wlad Kusnezow, Yana V Syagailo, Sven Rüffer, Konstantin Klenin, Walter Sebald, Jörg D Hoheisel, Christoph Gauer, and Igor Goychuk. Kinetics of antigen binding to antibody microspots: strong limitation by mass transport to the surface. *Proteomics*, 6(3):794–803, Feb 2006.

[32] Wlad Kusnezow, Yana V Syagailo, Igor Goychuk, Jörg D Hoheisel, and David G Wild. Antibody microarrays: the crucial impact of mass transport on assay kinetics and sensitivity. *Expert Rev Mol Diagn*, 6(1):111–24, Jan 2006.

[33] David M Rissin, Cheuk W Kan, Todd G Campbell, Stuart C Howes, David R Fournier, Linan Song, Tomasz Piech, Purvish P Patel, Lei Chang, Andrew J Rivnak, Evan P Ferrell, Jeffrey D Randall, Gail K Provuncher, David R Walt, and David C Duffy. Single-molecule enzyme-linked immunosorbent assay detects serum proteins at subfemtomolar concentrations. *Nature Biotechnology*, 28(6):595–599, Jan 2010.

[34] Jonghyun Go and Muhammad A Alam. Statistical interpretation of "femtomolar" detection. *Appl. Phys. Lett.*, 95(3):033110, Jan 2009.

[35] P.E Sheehan and L.J Whitman. Detection limits for nanoscale biosensors. *Nano Letters*, 5(4):803–807, Jan 2005.

[36] S Avrameas. Coupling of enzymes to proteins with glutaraldehyde:: Use of the conjugates for the detection of antigens and antibodies. *Immunochemistry*, Jan 1969.

[37] D Yorde, E Sasse, T Wang, and R Hussa. Competitive enzyme-liked immunoassay with use of soluble enzyme/antibody immune complexes for labeling. i. measurement of human choriogonadotropin. *Clinical ...*, Jan 1976.

[38] Electra Gizeli and Christopher R. Lowe. *Biomolecular sensors*. CRC Press, Jan 2002.

[39] F Schreiber. Self-assembled monolayers: from'simple'model systems to biofunctionalized interfaces. *Journal of Physics: Condensed Matter*, 16:R881, 2004.

[40] M Hegner, P Wagner, and G Semenza. Ultralarge atomically flat template-stripped au surfaces for scanning probe microscopy. *Surface Science*, 291(1-2):39–46, Jan 1993.

[41] P Gupta, K Loos, A Korniakov, C Spagnoli, M Cowman, and A Ulman. Facile route to ultraflat sam-protected gold surfaces by "amphiphile splitting". *Angewandte Chemie - International Edition*, 43(4):520–523, Jan 2004.

[42] R.G Nuzzo and D.L Allara. Adsorption of bifunctional organic disulfides on gold surfaces. *Journal of the American Chemical Society*, 105(13):4481–4483, Jan 1983.

[43] A Ulman. Formation and structure of self-assembled monolayers. *Chemical Reviews*, 96(4):1533–1554, Jan 1996.

[44] T Ekblad and B Liedberg. Protein adsorption and surface patterning. *Current Opinion in Colloid & Interface Science*, Jan 2010.

[45] E Ostuni, RG Chapman, RE Holmlin, S Takayama, and GM Whitesides. A survey of structure–property relationships of surfaces that resist the adsorption of protein. *Langmuir*, 17(18):5605–5620, 2001.

[46] MA Cooper. Optical biosensors in drug discovery. *Nature Reviews Drug Discovery*, 1(7):515–528, 2002.

[47] JA Camarero. Recent developments in the site-specific immobilization of proteins onto solid supports. *Peptide Science*, 90(3):450–458, 2008.

[48] L.S Wong, F Khan, and J Micklefield. Selective covalent protein immobilization: Strategies and applications. *Chemical Reviews*, 109(9):4025–4053, Jan 2009.

[49] M Kruppa and B Konig. Reversible coordinative bonds in molecular recognition. *Chem. rev*, 106(9):3520–3560, 2006.

[50] F Rusmini, Z Zhong, and J Feijen. Protein immobilization strategies for protein biochips. *Biomacromolecules*, 8(6):1775–1789, Jan 2007.

[51] C M Niemeyer, T Sano, C L Smith, and C R Cantor. Oligonucleotide-directed self-assembly of proteins: semisynthetic dna–streptavidin hybrid molecules as connectors for the generation of macroscopic arrays and the construction of supramolecular bioconjugates. *Nucleic Acids Res*, 22(25):5530–9, Dec 1994.

[52] E Hochuli, H Döbeli, and A Schacher. New metal chelate adsorbent selective for proteins and peptides containing neighbouring histidine residues. *J Chromatogr*, 411:177–84, Dec 1987.

[53] G.B Sigal, C Bamdad, A Barberis, J Strominger, and G.M Whitesides. A self-assembled monolayer for the binding and study of histidine-tagged proteins by surface plasmon resonance. *Analytical Chemistry*, 68(3):490–497, Jan 1996.

[54] Ramunas Valiokas, Goran Klenkar, Ali Tinazli, Annett Reichel, Robert Tampé, Jacob Piehler, and Bo Liedberg. Self-assembled monolayers containing terminal mono-, bis-, and tris-nitrilotriacetic acid groups: characterization and application. *Langmuir : the ACS journal of surfaces and colloids*, 24(9):4959–67, May 2008.

[55] Markus F Templin, Dieter Stoll, Monika Schrenk, Petra C Traub, Christian F Vöhringer, and Thomas O Joos. Protein microarray technology. *Trends Biotechnol*, 20(4):160–6, Apr 2002.

[56] R Maoz, SR Cohen, and J Sagiv. Nanoelectrochemical patterning of monolayer surfaces: toward spatially defined self-assembly of nanostructures. *Advanced Materials*, 11(1):55–61, 1999.

[57] CA Mirkin. The power of the pen: development of massively parallel dip-pen nanolithography. *ACS nano*, 1(2):79–83, 2007.

[58] K Lee, S Park, C Mirkin, J Smith, and M Mrksich. Protein nanoarrays generated by dip-pen nanolithography. *Science*, Jan 2002.

[59] R.D Piner, J Zhu, F Xu, S Hong, and C.A Mirkin. Âť Âťdip-pen" nanolithography. *Science*, 283(5402):661–663, Jan 1999.

[60] Ali Tinazli, Jacob Piehler, Mirjam Beuttler, Reinhard Guckenberger, and Robert Tampé. Native protein nanolithography that can write, read and erase. *Nature nanotechnology*, 2(4):220–5, Apr 2007.

[61] Cristian Staii, David W Wood, and Giacinto Scoles. Verification of biochemical activity for proteins nanografted on gold surfaces. *J Am Chem Soc*, 130(2):640–6, Jan 2008.

[62] Fouzia Bano, Ljiljana Fruk, Barbara Sanavio, Maximilian Glettenberg, Loredana Casalis, Christof M Niemeyer, and Giacinto Scoles. Toward multiprotein nanoarrays using nanografting and dna directed immobilization of proteins. *Nano Lett*, 9(7):2614–8, Jul 2009.

[63] Elham Mirmomtaz, Matteo Castronovo, Christian Grunwald, Fouzia Bano, Denis Scaini, Ali A Ensafi, Giacinto Scoles, and Loredana Casalis. Quantitative study of the effect of coverage on the hybridization efficiency of surface-bound dna nanostructures. *Nano Lett*, 8(12):4134–9, Dec 2008.

[64] Maozi Liu, Nabil A Amro, and Gang yu Liu. Nanografting for surface physical chemistry. *Annual review of physical chemistry*, 59:367–86, Jan 2008.

[65] Cristian Staii, David W Wood, and Giacinto Scoles. Ligand-induced structural changes in maltose binding proteins measured by atomic force microscopy. *Nano Lett*, 8(8):2503–9, Aug 2008.

[66] Matteo Castronovo, Slobodanka Radovic, Christian Grunwald, Loredana Casalis, Michele Morgante, and Giacinto Scoles. Control of steric hindrance on restriction enzyme reactions with surface-bound dna nanostructures. *Nano Lett*, 8(12):4140–5, Dec 2008.

[67] Yih Horng Tan, Maozi Liu, Birte Nolting, Joan G Go, Jacquelyn Gervay-Hague, and Gang yu Liu. A nanoengineering approach for investigation and regulation of protein immobilization. *ACS nano*, 2(11):2374–84, Nov 2008.

[68] C P Woodbury. *Introduction to Macromolecular Binding Equilibria*. CRC Press, Jan 2008.

[69] Wlad Kusnezow, Yana V Syagailo, Sven Rüffer, Nina Baudenstiel, Christoph Gauer, Jörg D Hoheisel, David Wild, and Igor Goychuk. Optimal design of microarray immunoassays to compensate for kinetic limitations: theory and experiment. *Mol Cell Proteomics*, 5(9):1681–96, Sep 2006.

[70] J.G Safar, M Scott, J Monaghan, C Deering, S Didorenko, J Vergara, H Ball, Giuseppe Legname, E Leclerc, L Solforosi, H Serban, D Groth, D.R Burton, S.B Prusiner, and R.A Williamson. Measuring prions causing bovine spongiform encephalopathy or chronic wasting disease by immunoassays and transgenic mice. *Nature Biotechnology*, 20(11):1147–1150, Jan 2002.

[71] G Binnig, CF Quate, and C Gerber. Atomic force microscope. *Physical review letters*, 56(9):930–933, 1986.

[72] Nuno Santos and Miguel Castanho. An overview of the biophysical applications of atomic force microscopy. *Biophys Chem*, 107(2):133–149.

[73] R Garcia and R Perez. Dynamic atomic force microscopy methods. *Surface science reports*, 47(6-8):197–301, 2002.

[74] G Cellot, E Cilia, S Cipollone, V Rancic, A Sucapane, S Giordani, L Gambazzi, H Markram, M Grandolfo, D Scaini, F Gelain, L Casalis, M Prato, M Giugliano, and L Ballerini. Carbon

nanotubes might improve neuronal performance by favouring electrical shortcuts. *Nature nanotechnology*, 4(2):126–133, Jan 2009.

[75] DM Eigler and EK Schweizer. Positioning single atoms with a scanning tunnelling microscope. *Nature*, 344(6266):524–526, 1990.

[76] S Xu and G.-Y Liu. Nanometer-scale fabrication by simultaneous nanoshaving and molecular self-assembly. *Langmuir*, 13(2):127–129, Jan 1997.

[77] S Xu, P.E Laibinis, and G.-Y Liu. Accelerating the kinetics of thiol self-assembly on gold - a spatial confinement effect. *J. Am. Chem. Soc.*, 120(36):9356–9361, Jan 1998.

[78] Denis Scaini, Matteo Castronovo, Loredana Casalis, and Giacinto Scoles. Electron transfer mediating properties of hydrocarbons as a function of chain length: a differential scanning conductive tip atomic force microscopy investigation. *ACS nano*, 2(3):507–15, Mar 2008. na.

[79] Ying Hu, Aditi Das, Michael H Hecht, and Giacinto Scoles. Nanografting de novo proteins onto gold surfaces. *Langmuir : the ACS journal of surfaces and colloids*, 21(20):9103–9, Sep 2005.

[80] M.A Case, G.L McLendon, Y Hu, T.K Vanderlick, and Giacinto Scoles. Using nanografting to achieve directed assembly of de novo designed metalloproteins on gold. *Nano Lett*, 3(4):425–429, Jan 2003.

[81] C You, M Bhagawati, A Brecht, and J Piehler. Affinity capturing for targeting proteins into micro and nanostructures. *Analytical and Bioanalytical Chemistry*, 393(6-7):1563–1570, Jan 2009.

[82] B Luginbühl, Z Kanyo, RM Jones, RJ Fletterick, SB Prusiner, FE Cohen, RA Williamson, DR Burton, and A Plückthun. Directed evolution of an anti-prion protein scfv fragment to an affinity of 1 pm and its structural interpretation. *Journal of molecular biology*, 363(1):75–97, 2006.

[83] R Zahn, A Liu, T Lührs, R Riek, C von Schroetter, F López García, M Billeter, L Calzolai, G Wider, and K Wüthrich. Nmr solution structure of the human prion protein. *Proc Natl Acad Sci USA*, 97(1):145–50, Jan 2000.

[84] R.A Williamson, D Peretz, C Pinilla, H Ball, R.B Bastidas, R Rozenshteyn, R.A Houghten, S.B Prusiner, and D.R Burton. Mapping the prion protein using recombinant antibodies. *Journal of Virology*, 72(11):9413–9418, Jan 1998.

[85] David R. Lide. Crc handbook of chemistry and physics. page 2828, Jan 2009.

[86] Luigi Calzolai and Ralph Zahn. Influence of ph on nmr structure and stability of the human prion protein globular domain. *J Biol Chem*, 278(37):35592–6, Sep 2003.

[87] R Riek, S Hornemann, G Wider, M Billeter, R Glockshuber, and K Wüthrich. Nmr structure of the mouse prion protein domain prp(121-321). *Nature*, 382(6587):180–2, Jul 1996.

[88] T Yang, O.K Baryshnikova, H Mao, M.A Holden, and P.S Cremer. Investigations of bivalent antibody binding on fluid-supported phospholipid membranes: The effect of hapten density. *Journal of the American Chemical Society*, 125(16):4779–4784, Jan 2003.

[89] G Schwarz and S Stankowski. Linear cooperative binding of large ligands involving mutual exclusion of different binding modes. *Biophys Chem*, 10(2):173–81, Sep 1979.

[90] G.P Saborio, B Permanne, and C Soto. Sensitive detection of pathological prion protein by cyclic amplification of protein misfolding. *Nature*, 411(6839):810–813, Jan 2001.

[91] A Kranjc, S Bongarzone, G Rossetti, X Biarnés, A Cavalli, M.L Bolognesi, M Roberti, Giuseppe Legname, and P Carloni. Docking ligands on protein surfaces: The case study of prion protein. *J. Chem. Theory Comput.*, 5(9):2565–2573, Jan 2009.

[92] Michele Vendruscolo, Jesús Zurdo, Cait E MacPhee, and Christopher M Dobson. Protein folding and misfolding: a paradigm of self-assembly and regulation in complex biological systems. *Philos Transact A Math Phys Eng Sci*, 361(1807):1205–22, Jun 2003.

[93] Marco Brucale, Massimo Sandal, Selena Di Maio, Aldo Rampioni, Isabella Tessari, Laura Tosatto, Marco Bisaglia, Luigi Bubacco, and Bruno Samorì. Pathogenic mutations shift the equilibria of alpha-synuclein single molecules towards structured conformers. *Chembiochem*, 10(1):176–83, Jan 2009.

[94] Isabella Tessari, Marco Bisaglia, Francesco Valle, Bruno Samorì, Elisabetta Bergantino, Stefano Mammi, and Luigi Bubacco. The reaction of alpha-synuclein with tyrosinase: possible implications for parkinson disease. *J Biol Chem*, 283(24):16808–17, Jun 2008.

thanks

I wish to express my endless gratitude and deepest affection to all the people that spontaneously, enthusiastically, intentionally and fortuitously, have been part of my life during these delightful, scrumptious years.